METHODOLOGY FOR THE DIRECTIONAL GROWTH OF CONDUCTING NANOWIRES AND THEIR ATTACHMENT TO LIVE CELLS

By

PREM THAPA

Bachelor of Science
Bangladesh Institute of Technology
Rajsahi, Bangladesh
1995

Master of Science
Oklahoma State University
Stillwater, Oklahoma
2002

Submitted to the Faculty of the
Graduate College of the
Oklahoma State University
in partial fulfillment of
the requirements for
the Degree of
DOCTOR OF PHILOSOPHY
December, 2008

METHODOLOGY FOR THE DIRECTIONAL GROWTH OF CONDUCTING NANOWIRES AND THEIR ATTACHMENT TO LIVE CELLS

Dissertation Approved:

Dr. Bret N. Flanders

Dissertation Adviser

Dr. Daniel R. Grischkowsky

Dr. John Mintmire

Dr. Bruce J. Ackerson

Dr. Jeffrey A. Hadwiger

Dr. A. Gordon Emslie

Dean of the Graduate College

ACKNOWLEDGEMENTS

At first, I would like to thank my adviser, Dr. Bret N. Flanders for giving me an opportunity to join his group and work on this project. Throughout the years of my study as a graduate student, I learned a lot from him. He always encouraged and advised me properly during experimental set-ups, manuscripts writing and paper presentations. I could not achieve this much without his support and guidance. Secondly, I would like to express my sincere gratitude to Dr. Jeffery Hadwiger, Associate Professor in Department of Microbiology, Oklahoma State University, who provided the cell culture facilities for my experiments. He has not only provided the cells for my research, but has always shared his expertise on the field of *Dictyostelium* cells to advise me. I appreciate him for many helpful comments and valuable suggestions on my experiments. Thirdly, I would like to thank Professor Dr. Daniel R. Grischkowsky for providing lithographic chips without which this work would not have been possible. It is my pleasure to thank Dr. Daniel Grischkowsky, Dr. Bruce Ackerson, Dr. Jeffery Hadwiger and Dr. John Mintmire for their time as members of my advisory committee.

In addition, I would like to thank my former lab members Birol Ozturk, Ishan Talukdar, Joel DeWitt and Srinivasan Vennupasa for their contributions to this work. They are marvelous people with whom I shared much in the way of good humor, scienti-

fic discussions and good friendship. This company never let me feel bored at lab and were always ready to help me in my lab works.

Finally, I would like to thank my beloved wife, Jhunu who always loves and supports me all the time. I am grateful to my parents, who have provided me with a happy and meaningful life. My son Sayuz and daughter Sejal is also a source of motivation for my successful research.

TABLE OF CONTENTS

Chapter Page

LIST OF TABLES

Table Page

LIST OF FIGURES

CHAPTER I

INTRODUCTION

The effort to develop applications for the nanoscientific findings of the past 3 decades has been largely directed towards small scale electronics and circumvention of Moore's law. However, the past 5 years have seen significant interest grow in the alternative area of nanostructural probes and sensors for biological molecules, cells, and tissues. Integrating nanotechnology with experimental biology could lead to techniques for making measurements on biological systems with enhanced spatial resolution. There is growing interest in performing single cellular and sub-cellular experimentation and manipulation such as: single-cell surgery, localized drug release, and spatially resolved cell monitoring. [32, 33, 34] On this development, researchers have already showed the possibility of electrical detection of variety of biological molecules using carbon nanotube-based materials,[35] exemplifying biological probing through a nano-technological approach. An important example is the utilization of nanowire-based transistors for electrical detection of specific biomolecules.[36, 37, 45] Of fundamental importance in this biological stimulation and sensing arena is the development of techniques for attaching electrodes to living cells and tissues. Development on this front is expected to generate new knowledge of the complex regulatory and signaling pathways

That underlie cellular behavior. The attainment of this goal requires, electrodes with submicron dimensions in order to interface with individual cellular and sub-cellular targets. Hence, one feels compelled to look to recent progress in nanotechnology for elegant, new approaches to surmounting this technological challenge. This thesis will delineate a new nanowire growth technique that is well-suited to this challenge.

It is useful to attach electrodes to living cells because biological cells are electrical objects. This character may be understood as follows. Biological cells have membranes made of lipid bilayer, that serves as a barrier to the passage of most polar molecules. The cytoplasm contains a high concentration of solutes that are not present in the exoplasm. Many of these are negatively charged organic molecules (anions) and their accompanying counter-ions (cations). Thus, at thermal equilibrium, a cell would suffer severe osmotic imbalance and would likely burst. To combat this tendency, cells have machinery that actively pumps out inorganic ions in order to attain osmotic balance. The best understood is the Na^+- K^+ pump, which drives 3 Na^+ ions out of the cell for 2 K^+ ions into the cell for every ATP molecule that phosphorylates it.[16] Thus, ion-pumping reduces the cytoplasmic solute concentration by (net) one cation per cycle, reducing the osmotic imbalance. Ion pumping also endows the cell with one negative charge per cycle. Figure I.1, illustrates the make-up of these salt solutions, where the concentration of K^+ ions is higher inside the membrane than outside and the opposite is true for Na^+ and Cl^- ions. The slight difference in electrical charge on the two sides of a cell membrane gives rise to the membrane potential. This feature is mainly due to differences between

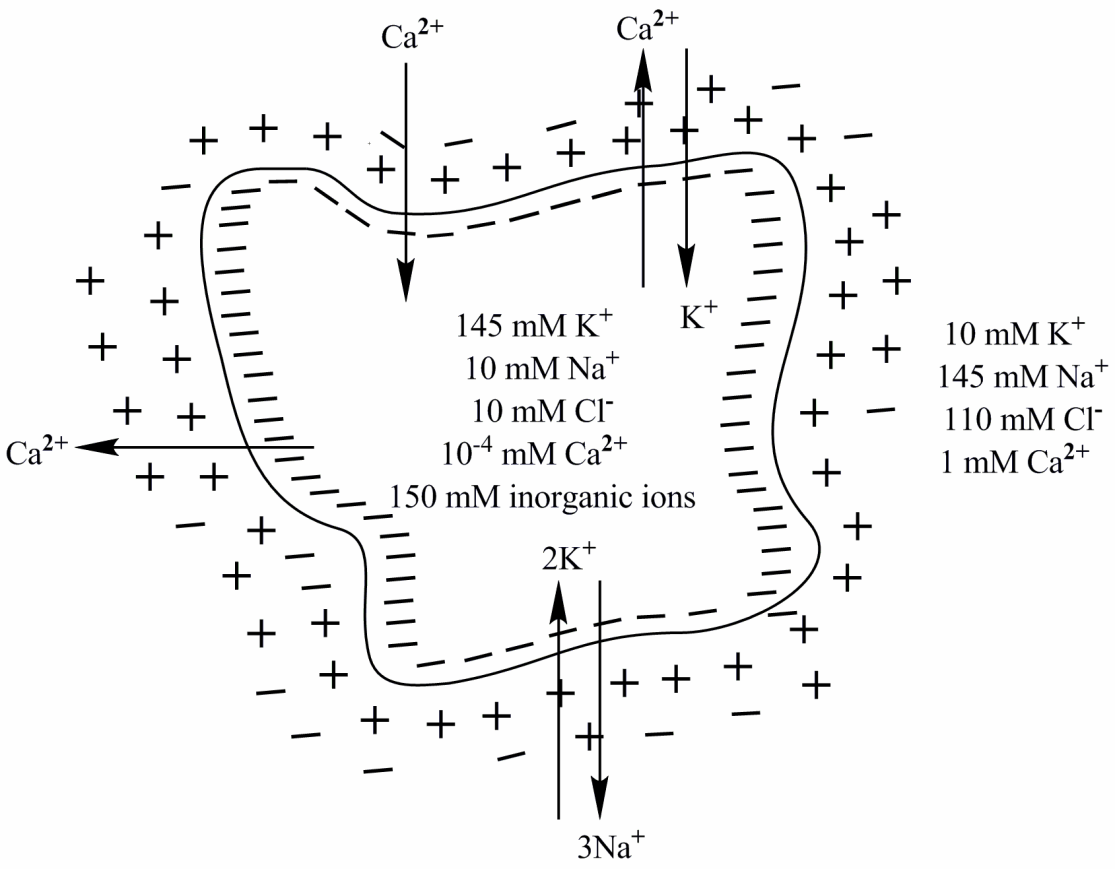

Figure I.1. The distribution of ions and solutes inside and outside the cell membrane and the function of Na^+- K^+ pump and ion exchanger for ion exchange through ion channels.

the Na^+, K^+, Ca^{2+}, and Cl^- concentration outside and inside the cell. The potential difference, $\Delta\phi$ that exists across the membranes of excitable cells is ~ -60 mV,[20] or even larger depending on cell type.

The differences between the intra and extracellular concentrations of a particular species create Nernst potentials V_i:

$$V_i = -\frac{\kappa_B T}{e} \ln \frac{C_{2,i}}{C_{1,i}} \qquad \text{(I.1)}$$

Where, the subscript i indicates the species of interest, k_BT is the thermal energy, e is the (positive or negative) charge of the species, and $C_{2,i}$ and $C_{1,i}$ are the cytoplasmic and exoplasmic concentrations of species i. In many cell types, the Nernst potentials for K^+ (-67 mV) and Cl^- (-60 mV) are similar to the membrane potential, while those for Na^+ (67 mV) and Ca^{2+} (115 mV) are much more positive than the membrane potential. These quantities are shown in table I.1. All cells have a sodium anamoly of this type. The electrochemical driving force that a particular type of ion feels is the difference in membrane potential $\Delta\phi$ and Nernst potential V_i, available to move the ion across the membrane. Both the Nernst and membrane potentials will drive a flux of ionic species i that is proportional to the conductance per area g_i (of membrane) for that species.

$$\downarrow = ((- \downarrow) \downarrow$$

(I.2)

This electrochemical potential is used to drive *transient* fluxes of particular types of small ions (usually Cl^-, Na^+, and Ca^{2+}) across the membrane. These fluxes occur at specific structures in the cellular membrane called ion channels. The ion channels are specialized proteins that are present in the cell membrane and form pores. They perform three important properties: 1) allow the movement of ions across the cell membrane, 2) select specific ions and, 3) open and close in response to specific stimuli: electrical, mechanical or chemical.[46]

Ions	Intracellular Concentration, (mM)	Extracellular Concentration, (mM)	Membrane Potential, (mV)	Nernst Potential, (mV)	Driving Force (mV)
K^+	145	10	-60	-67	7
Na^+	10	145	-60	+67	-127
Cl^-	10	110	-60	-60	0
Ca^{2+}	10^{-4}	1	-60	+115	-175

Table I.1. A comparision of ion concentration, Nernst potential and driving force inside and outside of a typical Mammalian Cell.[16]

In order to make precise studies of these cellular processes, it is necessary to be able to stimulate single ion channels at user-chosen sites on an individual cell. This goal requires methodology for attaching electrodes to targeted cells. The leading technology for studying these trans-membrane current in live cells is the patch-clamp technique,[10, 16] which was invented by Sakmann and Neher in 1976. In this technique, the microtip of the glass pipette is attached to the membrane and a small section of it (only one ion channel) is sucked out. This technique is capable of measuring ion fluxes through a single channel and provides a direct way to attach an electrode to a user-chosen site on the cellular membrane.[10] The density of these ion channels in *Dictyostelium* cell is about 0.1 μm^{-2} for DI and HI channel and 0.02 μm^{-2} for the DII channels.[56]

While affording the (expert) user a high degree of control over the location (on the cell) of the contact point, the nature of this contact is strongly perturbative to the cell: the user-enforced mechanical coupling between the pipette-tip and the cell is known to stretch the membrane, and, thereby, induce the leakage of ions across the membrane.[62, 63] An improved approach to bringing a conducting electrode into contact with a cell would be to induce the cell to attach itself or, even better, a selected sub-section of itself, to the electrode. In such an approach, the most perturbative steps of the patch clamp technique could be circumvented.

Dictyostelium discoideum are single celled amoebae that grow in nutrient-rich environments, and that migrate with the extension of pseudopodia in response to pulses of folic acid and cyclic AMP.[28] By migrating up the concentration gradients of these

chemicals, a process called chemotaxis, these cells undergo directional migration. When the *Dictyostelium* cells are starved for several hours, the cells secrete an extracellular adenosine 3', 5'-cyclic mono-phosphate (cAMP), which is then relayed from cell to cell. The surface of the cell membrane consists of chemoattractant receptors (CAR1-CAR4), which bind cAMP, then couple to the G-proteins (α, β, γ) as illustrated in Figure I.3. The secondary messengers guanyl cyclase (GC), phospholipase C (PLC), and adenyl cyclase (AC) are activated when the receptors are reduced. The PI3K proteins (lipid kinases) phosphorylate the phosphotidyl-inositol triphosphate PI(3, 4, 5)P_3, which is accumulated at the leading edge of the cell. The accumulation of PI(3, 4, 5)P_3 leads to F-actin polymerization and the protrusion of pseudopodia. The PI-3-Phosphotase (PTEN) plays an important role in degradation of PI(3, 4, 5)P_3 by the dephosphorilation of the lipid. PTEN remains bound to the posterior end of the membrane where myosin II is congregated into contractile filaments. The accumulation of myosin II suppress pseudopod formation and enhances retraction of the cell's posterior.[43] The movement of these cells results from a combination of actin polymerization at the front end and myosin contraction at the rear end of the cell. [39]

Many types of cells respond to direct-current electric fields by directional migration, which is called electrotaxis. The *Dictyostelium* cells and corneal epithelial cells migrate to the negative electrodes, whereas they avoid positive electrodes.[21] These kind of motile cells show directional migration and cell aggregation in response to

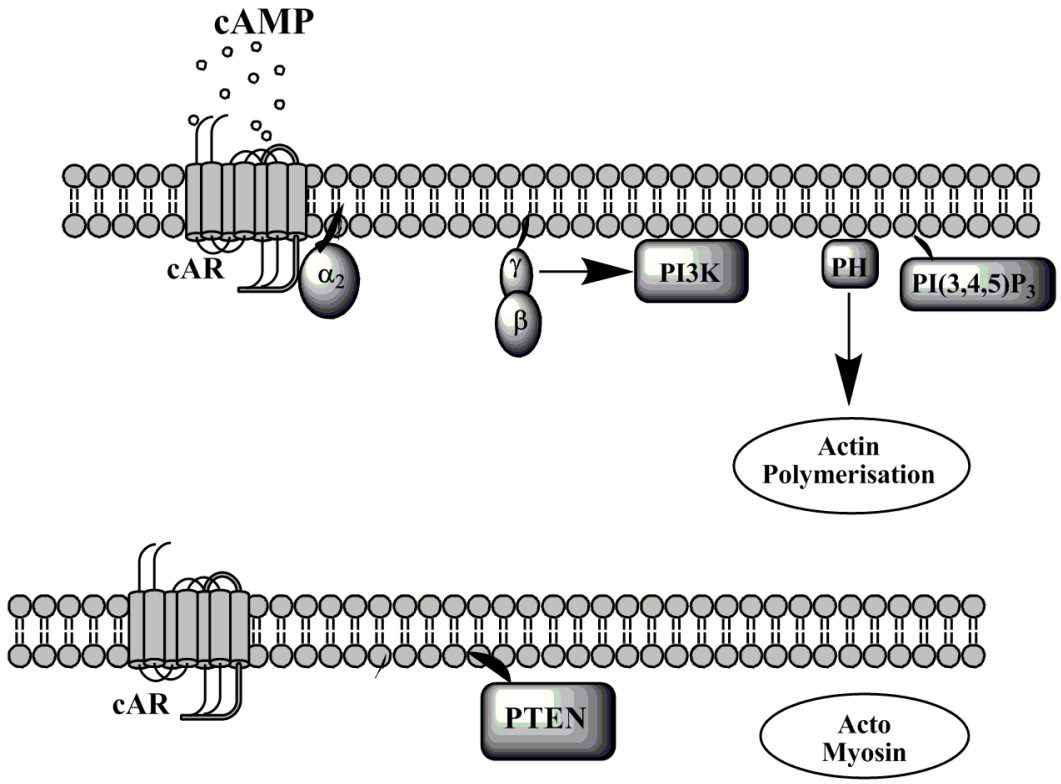

Figure I.3. cAMP receptor mediated signaling pathways of *Dictyostelim* cell. The model shows intracellular signaling to produce PIP_3 and F-actin polymerisation at the top and PTEN and acto-myosin at the bottom.[24]

electric fields.[44] The electrotactical migration of *Dictyostelium* cells bears some similarity to their chemotactical migration. However, there are important differences between the underlying signaling mechanisms for these migration-modes. As described above most chemoattractants act through G protein-linked signaling pathways to mediate directional migration in chemotaxis, however the Gβ–null mutations still perform reduced electrotaxis in *Dictyostelium* cells; thus, G-proteins are likely involved in electrotaxis in only a secondary manner.[44] Further work is required to gain a detailed understanding of these electrotactical signaling mechanisms.[60, 61] Despite the uncertainty regarding the details of this mechanism, the electrotactical behavior suggests that strategically applied electric fields may be used to induce the cells to migrate towards and make contact with electrodes that are immersed in the cellular environment. This approach to achieving cell-to-wire contacts would, likely, be only weakly perturbative to the cell as the contact is made by the cell, rather than enforced by the user.

Our group has developed a method to grow individual conducting nanowires between targeted points in external circuitry. [14, 17, 18] The approach is straight-forward, simply requiring the application of alternating voltage signals to simple salt solutions. This technique is called *Directed Electrochemical Nanowire Assembly* (DENA), which has a number of nice properties that enable the precise addition of nanowires to on-chip circuitry. First, this technique enables the growth of near single crystalline, metallic nanowires.[14] Additionally; the nanowire diameter can be tuned by controlling the applied voltage frequency.[14] These wires are grown in user specified directions across distances of ~100 μm. The wire composition can be chosen from a wide variety of metals

including In, Au, Ni, Co, Ag, Pb, Pd,[47] and conducting polymers poly pyrrole, and poly thiophene.[64] There is potential to enable self wire-cell attachment by the migration of *Dictysostelium discoidium* cell to the negatively biased nanowire grown by DENA technique. This soft process of wire-cell attachment reduces the chance of rupturing the cell membrane and enhances the electrical contact between the wire and the cell membrane.

This thesis establishes new methodology for attaining strong cell-to-wire contacts at specific sub-cellular sites in a manner that is only weakly perturbative to the living cells. To fabricate electrodes of the correct dimension and for interfacing with individual submicron features of a cell, we have developed methodology for growing conducting polymer nano-wires from microscopic electrodes on the cell supporting-substrates. These nanostructured polymeric electrodes are prepared electrochemically, so knowledge of the voltage-profile in the electrolytic solution is critical to the rational application of this approach. Therefore, we present theory that describes the voltage-profile during wire-growth. Because this profile has a long range component that defines the growth path of the nanowire, precise control over the placement of the nanowire in the on-chip circuitry is attained. A future application that these novel cell-wire contact systems enable is mechanical (i.e. migratory) response of the cells to known voltage-stimuli, a critical sub-process of wound healing in mammalian epithelial tissues.

REFERENCES

1. Berridge, M.J., Bootman, M.J. & Lipp, P. Calcium-a life and death signal. Nature **395,** 645-648 (1998).

2. Pfitzer, G. et al. in *Molecular and Cellular Aspects of Muscle Contraction* 89-99 (2003).

3. Steger, K.A. & Avery, L. The GAR-3 muscarinic receptor cooperates with Calcium signals to regulate muscle contraction in the Caenorhabditis elegans pharynx. *Genetics* **167**, 633-643 (2004).

4. Canaff, L. & Hendy, G. N. Calcium-sensing receptor gene transcription is up-regulated by the proinflammatory cytokine, interleukin-1 beta – Role of the NF-κβ pathway and κβ elements. *Journal of Biological Chemistry* **280,** 14177-14188 (2005).

5. Basta-Kaim, A. et al. Chlorpromazine inhibits the glucocorticoid receptor-mediated gene transcription in a calcium-dependent manner. *Neuropharmacology* **43**, 1035-1043 (2002).

6. Meldolesi, I. Surface wound healing: a new, general function of eukaryotic cells. *Journal of Cellular and Molecular Medicine* **7**, 197-203 (2003).

7. Yoshida, H., Nobe, K., Nobe, H., Paul, R.J. & Honda, K. Calcium-dependent and Independent signaling pathways are involved in thromboxane A(2)-induced fibroblast contraction in wound healing. *Journal of Pharmacological Sciences* **97**, 201P-201P (2005).

8. Nunemaker, C. S. et al. Islet calcium oscillations differ from mouse to mouse in vitro but correlate with insulin secretion in vivo. *Diabetes* **54**, A412-A412 (2005).

9. Cruz-Cruz, R., Salgado, A., Sanchez-Soto, C., Vaca, L. & Hiriart, M. Thapsigargin- sensitive cationic current leads to membrane depolarization, calcium entry, and insulin secretion in rat pancreatic beta-cells. *American Journal of Physiology-Endocrinology and Metabolism* **289**, E439-E445 (2005).

10. Neher, E. & Sakmann, B., "The patch clamp technique," *Sci. American*, 44-51 1992).

11. Bootman, M. D. & Berridge, M. J., "The elemental principles of calcium Signaling," *Cell*, **83**, 675-678 (1995).

12. Lipp, P. & Niggli, E., " A hierarchical concept of cellular and subcellular Ca^{2+} Signaling," *Prog.Biophys. Mol. Biol*., **65**, 265-296 (1996).

13. Pucovsky, V., Gordienko, D. V. & Bolton, T. B. "Effect of nitric oxide donors and Noradrenaline on Ca^{2+} release sites and global intracellular Ca^{2+} in myocytes from gunea-pig small mesenteric arteries". *J. Physiol*. **539.1**, 25-39 (2002).

14. Ozturk, B., Talukdar, I., & Flanders, B. N., "Directed growth of diameter-tunable Nanowires", *Nanotechnology* **18 (***2007).*

15. Skotheim, T. A. & Reynolds, J. R. *Handbook of Conducting Polymers* (Boca Raton, London, 2007).

16. Albert, B., Johnson, A., Lewis, J., Raff, M., Roberts, K. & Walter, P. (Molecular Biology of the Cell, 2002).

17. Talukdar, I., Ozturk, B., Mishima, T. D. & Flanders, B. N., "Directed Growth of Single-Crystal Indium Wires". *Applied Physics Letters*, 2006, **88**: p. 221907.

18. Ozturk, B., Mishima, T. D., Grischkowsky, D. R. & Flanders, B. N., "Single-Step Growth and Low Resistance Interfacing of Gold Nanowires". *Nanotechnology 2007.* **18**: p. 175707.

19. Bockris, J. & Reddy A. K. N. (Modern Electrochemistry, Plenum Press, New York, 1973).

20. Nelson, P. (Biological Physics, W. H. Freeman and Company, New York, 2004).

21. Shanley, L. J., Walczysko, P., Bain, M., MacEwan, D. J., & Zhao, M., "*Influx of extracellular Ca^{2+} is necessary for electrotaxis in Dictyostelium,*" J. Cell. Sci., **119**, 4741-4748 (2006).

22. Bock, G. R. & Ackrill, K. (1995) *Calcium Waves, Gradients, and Oscillations* (John Wiley & Sons, Chichester).

23. Richardson, S. M., Hendricks, J. L., & Martin D. C., "Electrochemical Polymerization of Conducting Polymers in Living Neural Tissue". *J. Neural Eng.* **4** (2007): L6-L13.

24. Willard, S. S., & Devreotes, P. N., "Signaling Pathways Mediating Chemotaxis In the Social Amoeba, *Dictyostelium discodeum*" *European Journal of Cell Biology,* **85** 897-904 (2006).

25. Qui, Y. J., Reynolds J. R., "Electrochemically Initiated Chain Polymerization of Pyrrole in Aqueous Media" *Journal of Polymer Science* **30,** 1315-1325 (1992).

26. Sadki, S., Schottland, P., Brodie, N., & Sabouraud, G., "The Mechanism of Pyrrole Electropolymerization" *Chem. Soc. Rev.,* **29** 283-293 (2000).

27. Genies, E. M., Bidan, G., & Diaz, A. F., "Spectroelectrochemical Study of Polypyrrole Films " *J. Electroanal. Chem.,* **149** 101 (1983).

28. Aubry, L., & Firtel, R., "Integration of Signaling Networks That Regulate Dictyo-Stelium Differentiation" *Annu. Rev. Cell. Dev. Biol.,* **15:** 469-517 (1999).

29. Ouyang, J., Chu, C. W., Chen, F. C., Xu, Q., & Yang, Y., "High-Conductivity PEDOT: PSS Film and Its Application in Polymer Optoelectronic" *Adv. Funct. Mater.,* **15:** No. 2 (2005).

30. Langridge, P. D., & Kay, R. R., "Blebbing of Dictyostelium Cells in Response to Chemoattractant" *Experimntal Cell Research*., **312:** 2009-2017 (2006).

31. Yoshida, K,. & Soldati, T., "Dissection of Amoeboid Movement into Two Mechanically Distinct Modes" *Journal of Cell Science* **119**: 3833-3844 (2006).

32. Britto, P., Santhanam, K., & Ajayan, P., *Bioelectrochem. Bio energ* **41:** 121(2005)

33. Fei, S., Chen, J., Yao, S., Deng, G., He, D., & Kuang, Y., *Anal. Biochem.* **339** 29 (2005).

34. Chen, R., Bangsaruntip, S., Drouvalakis, K., Wong, N., Kam, S., Shim, M., Li, Y., Kim, W., Utz, P., & Dai, H., *PNAS* **100:** 4984 (2003).

35. Kooklin, N., A., Kim, W., E., Lazoreck, A, D., & Xu, J., M., *Applied Physics Letters* **87:** 173901 (2005).

36. Zheng, G., F., Patolsky, F., Cui, Y., Wang, W., U., & Lieber, C., M., *Natl. Biotechnol.* **23:** 1294-1301 (2005).

37. Hahm, J., & Lieber, C., M., *Nano Lett.* **4:** 51-54 (2004).

38. Parent, C., A., & Devreotes, P., N., *Science* Vol: **284** (1999).

39. Kunito, Y., & Thierry, S., *Journal of Cell Science* **119:** 3833-3844 (2006).

40. Van, D., J., Ypey, D. L., & Van der Molen, L. G., "Electrophysiological properties Of Dictyostelium derived from membrane potential measurements with micro-Electrodes". *J. Membr. Biol.* **106:** 123-134 (1988).

41. Sasaki, T., A., Firtel, A., *European Journal of Cell Biology* **85:** 873-895 (2006).

42. Firtel, A., R., *Genes & Development* **9:** 1427-1444 (1995).

43. Franca-Koh, J., Kamimura, Y., & Devreotes, P., *Current Opinion in Genetics & Development* **16:** 333-338 (2006).

44. Zho, M., Jin, T., McCaig, C., D., Forrester, J., V., & Devreotes, P., N., *The Journal of Cell Biology* **157:** 921-927 (2002).

45. Patolsky, F., B. P. T., Yu, G., Fang, Y., Greytak, A. B., Zheng, G., & Lieber, C. M., "Detection, Stimulation, and Inhibition of Neuronal Signals with High-Density Nanowire Transistor Arrays." *Science*, **313:** 1100-1104 (2006).

46. Kandel, R. E., Schwartz, J. H., & Jessell, T. M., Essentials of Neurol Science And Behavior (McGraw-Hill Professional, 1995).

47. Cheug, C., Gonela, R. K., Gu, Q., & Haynie, D. T., *Nano Letters,* **5**, 175-178 (2005).

48. Laporte, C., Kosta, A., Klein, G., Aubry, L., Lam, D., Tresse, E., Luciani, MF., & Golstein, P., " A Necrotic Cell Death Model In a Protist" *Cell Death and Differentiation*, **14:** 266-274 (2007).

49. Charest, G. P., & Firtel, R. A., " Feedback Signaling Controls Leading-Edge Formation During Chemotaxis" *Current Opinion in Genetics & Development*, **16:** 339-347 (2006).

50. Franca-Koh, J., Kamimura, Y., & Devereotes, P., "Navigating Signaling Networks: Chemotaxis in Dictyostelium discoideum", *Current Opinion in Genetics & Development*, **16:** 333-338 (2006).

51. Kim, J., Van Haastert, P., & Devreotes, P. N., " Social Sciences: G-Protein Coupled Receptor Signaling Pathways in Dictyostelium discoideum", *Chemistry & Biology*, **3:** 239-243 (1996).

52. Keizer-Gunnink, I., Kortholt, A., & Van Haastert, P. J. M.,"Chemoattractants and Chemorepellents act by Inducing Opposite Polarity in Phospholipase C and PI3-Kinase Signaling", *The Journal of Cell Biology*, **177:** 579-585 (207).

53. Zhao, M., McCaig, D. C., Agius-Fernandez, A., Forrester, J. V., & Araki-Sasaki, K., "Human Corneal Epithelial Cells Reorient and Migrate Cathodally in a Small Applied Electric Field", *Current Eye Research*, 1997.

54. Kim, D. H., Richardson-Burns, S. M., Hendricks, L., Sequera, C., & Martin, D. C. "Effect of Immobilized Nerve Growth Factor on Conductive Polymers: Electrical Properties and Cellular Response", *Adv. Funct. Mater.* **17:** 79-86 (2007).

55. Richardson-Burns, S. M., Hendricks, J. L., Foster, B., Povlich, L. K., Kim, D. H., & Martin D. C., "Polymerisation of The conducting Polymer Poly (3,4-ethylenedioxythiophene) (PEDOT) Around Living Neural Cells", *Biomaterials,* **28:** 1539-1552 (2006).

56. Hartung, K., & Muller, U., " Properties of Three Different Ion Channels in the Plasma Membrane of the Slime Mold Dictyostelium discoideum", *Biochimica et Biophysica Acta,* **1026:** 204-212 (1990).

57. Galbraith, G., C., & Sheetz, P., M., " A Micromachined Device Provides a New Bend on Fibroblast Traction Forces" *Proc. Natl. Acad. Sci.* **94:** 9114-9118 (1997).

58. Harris, A., Wild, P., & Stopak, D., "Silicone Rubber Substrata: A New Wrinkle in the study of Cell Locomotion" *Science* **208:** 177-179 (1980).

59. Harris, A., Stopak, D., & Wild, P., "Fibroblast Traction as a Mechanism for Collagen Morphogenesis" *Nature* **290:** 249-251 (1981).

60. Zho, M., Bai, H., Wang, E., Forrester, J. V., & McCaig, D. C., "Electrical Stimulation Directly Induces pre-Angiogenic Responses in Vascular Endothelial Cells by Signaling Through VEGF Receptors." *Journal of Cell science,* **117:** 397-405 (2004).

61. McCaig, D. C., Rajnicek, A. M., Song, B., & Zhao, M., "Controlling Cell Behavior Electrically: Current Views and Future Potential." *Physiol Rev,* **85:** 943-978 (2005).

62. Ji, G., Feldman, R. J., & Kotlikoff, M. E., "Stretch-Induced Calcium Release in Smooth Muscle." *J. Gen. Physiol.* **119:** 533-544 (2002).

63. Perozo, E., Kloda, A., Cortes, D. M., & Martinac, B., "Physical Principles Under Lying the Transduction of Bilayer Deformation Forces During Mechanosensitive Channel gating." *Nature Structural Biology* **9:** 696-703 (2002).

64. Thapa, P. S., Barisci, J. N., Yu, D.J. et al., "Directional Growth of Conducting Polypyrrole and Polythiophene nanowires," *Appl. Phys. Lett.* **Submitted** (2008).

CHAPTER II

Directional growth of conducting polypyrrole and polythiophene wires

(Abstract

This work establishes an innovative electrochemical approach to the template-free growth of conducting polypyrrole and polythiophene wires along predictable, inter-electrode paths up to 30 μm in length. These wires have knobby structures with diameters as small as 98 nm. The conductivity of the polypyrrole wires is 0.5 ± 0.3 S cm^{-1}, while that of the polythiophene wires is 7.6 ± 0.8 S cm^{-1}. The control over the growth-path has enabled the growth of *electrode-wire-target* assemblies where the target is a microscopic sample such biological cell that is positioned in the inter-electrode gap. Such assemblies are of potential use in cell-stimulation studies.

II.1 Introduction

Conducting polymer nanowires are a burgeoning subfield of the polymeric electronics arena.[1] On a fundamental level, these wires serve as a testing ground for 1D transport theories that describe the Luttinger liquid[2] and Wigner crystal phases of electronic materials.[3] In sensor-applications, where analyte-binding to porous wires modulates the resistance of *electrode-wire-electrode* assemblies, polymeric wires are

exploited for their unusual combination of properties—conductivities as large as 2×10^2S cm^{-1},[4] and a high degree of porosity. As such, impressive sensitivities have been attained: sub-microbar pressures of ammonia, nanomolar concentrations of DNA,[5] and ~10 fM concentrations of micro-RNA[6] have been detected with these devices. Finally, polymeric wires are promising electrophysiological materials. A recent study has demonstrated the electropolymerization of polythiophene filaments within living neural tissue without compromising the viability of the surrounding neurons—a preliminary step towards remotely stimulating cells and tissue.[7, 8] A general requirement for all of these applications is the reproducible fabrication of electrode-wire-*target* assemblies, where the wire connects a user-selected electrode to a targeted site (*i.e.* a second electrode or a biological cell), enabling diagnostic instrumentation to be interfaced with the wire or target. Therefore, new methodologies for the *directional* growth of polymeric wires are of significant interest.

Templated growth techniques are in wide-use as they yield reproducible wire-shapes and wire-growth along predictable paths. To fabricate electrode-wire-electrode assemblies, this approach has been modified to enable electrodeposition of the polymer in prefabricated channels that connect user-chosen pairs of micro-electrodes.[9, 10] Thus, directional growth is realized by engineering growth-channels before electrochemically depositing the wire. To circumvent this step, template-free approaches have been developed where the growth of poly-aniline[5] and polythiophene[11] nanowires occurs between the tips of two electrodes; however, the maximum wire-length that was attained by these techniques was limited to < 10 μm. Dip-pen lithography relaxes the wire-length

constraint and provides excellent control over the positioning of the wires,[12] but is restricted to applications where the use of a scanning probe is feasible. To broaden the range of situations in which directional polymeric wire-growth is possible, the present work establishes a simple approach to growing conducting polymer wires across distances as large as 30 μm in on-chip circuitry to produce *electrode-wire-target* assemblies, where the target is either a second electrode or a biological cell.

To attain this goal, we have extended the *directed electrochemical nanowire assembly* (DENA) technique to the growth and interconnecting of polypyrrole and polythiophene wires. This technique has previously been used to grow *metallic* nanowires,[13-15] where an alternating voltage reduced and deposited metallic cations onto a biased electrode that was immersed in aqueous salt solution.[13] A similar approach is used here to electrochemically polymerize conducting polymer onto biased electrodes immersed in aqueous monomer solution, enabling the growth of polymeric electrode-wire-target assemblies. To our best knowledge, this effort demonstrates the first electrode-wire-target fabrication-method in which the growth-path is definable over tens-of-microns distances without an external mechanical apparatus, such as a channel or a scanning probe.

II.2 Experimental Setup

Figure II.1a depicts the simple wire-growth apparatus. The optical micrograph shows the electrode array used for wire-growth from aqueous pyrrole solution. The gap between the opposing tips is 18.8 μm. The electrodes were composed of 100 nm thick

base layers of Ti and 500 nm thick top layers of Au that were deposited on fused silica substrates using standard lithographic techniques.[16] A 10 μl aliquot of aqueous solution containing 0.50 M freshly distilled pyrrole and 0.50 M sodium dodecyl sulfate (SDS) was deposited across the electrodes. The pyrrole and SDS concentrations may be varied across the 0.05 M to 0.50 M range, and *p*-toluene sulfonate may be used instead of SDS as the anionic dopant. To induce wire-growth, a square-wave voltage-signal (± 3 V, 250 kHz) with a 50% duty cycle was applied to the left electrode while the right electrode was grounded. Growth was stopped by turning off the voltage when the wire reached the opposing electrode. This process was observed on an inverted microscope (Leica, IRB). The resulting electrode-wire-electrode assembly is shown in Figure II.1a. A transmission electron micrograph of a polypyrrole wire-segment is shown in the inset. The wire has a knobby structure with a lengthwise averaged diameter of 560 nm.

Milder conditions may be used to grow wires from aqueous thiophene solutions. The fiber in Figure II.1b was grown by depositing 10 μl of aqueous solution containing 0.01 M ethylenedioxy-thiophene (EDOT) and 0.02 M poly(sodium styrene sulfonate) (PSS) across the electrodes. Additionally, a smaller voltage-amplitude (± 2.5 V) and frequency (100 kHz) were used to induce growth. The inter-electrode gap in Figure II.1b is 30.2 μm. The inset depicts a scanning electron micrograph of the wire. As with the polypyrrole wire, its structure is knobby, varying from 98 to 669 nm in thickness with a lengthwise averaged diameter of 340 nm.

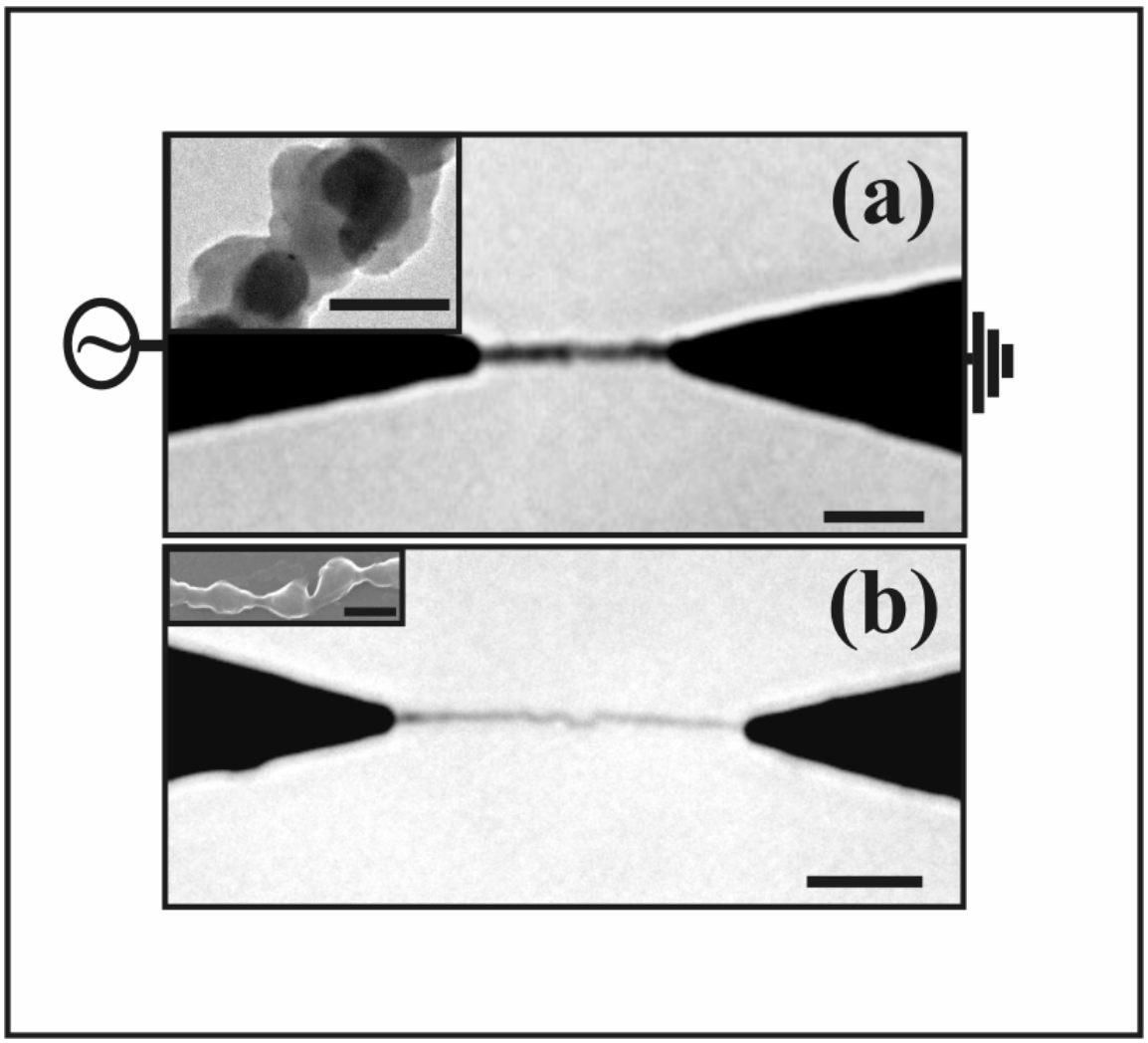

Figure II.1: (**a)** The DENA apparatus for growing polymeric wires. The optical micrograph shows a wire grown from aqueous pyrrole/SDS solution. The scale bar denotes 10 μm. **Inset:** A TEM micrograph of a polypyrrole wire-segment. The wire was broken free of the electrodes and deposited on a grid for imaging in a LaB_6 JEOL JEM 2100 microscope. The scale bar denotes 500 nm. (**b)** An optical micrograph of a wire grown from aqueous EDOT/PSS solution. The scale bar denotes 10 μm. **Inset:** An SEM micrograph of a polythiophene nanowire. The scale bar denotes 500 nm; imaging was performed on a FEI Quanta 600 FEG.

II.3 Results and Discussion

As Figures II.1a & II.1b illustrate, the growth-path is predictable: it follows the tip-to-tip line between the user-selected electrodes as a result of applying an alternating voltage to one electrode and grounding the other. This path is defined by the voltage-profile in the solution, but a full description of the underlying ionic diffusion and screening behavior will be described in next chapter.

The compositions of the DENA-grown wires were determined by micro-Raman spectroscopy. Wire-laden electrode arrays were prepared as described above and transferred to the spectrometer (Jobin Yvon, U1000). Wires grown from pyrrole-solutions were characterized by illuminating the wire-segments with 1.5 mW of 632.8 nm laser radiation, which was focused to a 2.0 μm spot size, the monochrometer-entrance slit was set to 200 μm wide. A typical spectrum is shown in Figure II.2a (filled circles) and compared to the spectrum of a polypyrrole film (solid line) that was prepared by a standard protocol[17, 18]. The small intensity-differences are due to the sensitivity of the micro-Raman technique to the laser-spot position on the sub-micron sample. Moreover, both spectra exhibit features that are characteristic of polypyrrole: peaks at 1050 cm^{-1} (the symmetrical CH-in-plane bending mode), at 1310 cm^{-1} and 1375 cm^{-1} (the anti-symmetrical CH-in-plane bending mode), and at 1600 cm^{-1} (the C=C stretching mode);[18] hence, the DENA-grown wire is composed of polypyrrole.

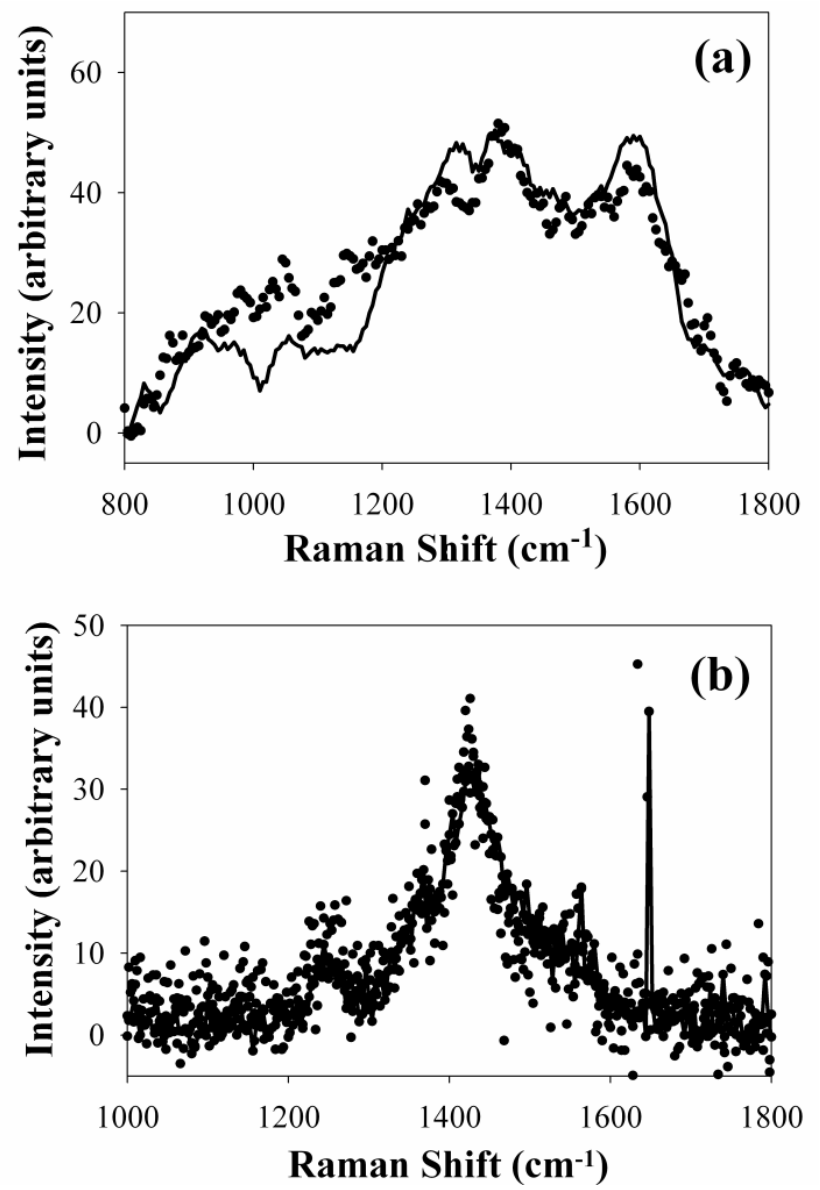

Figure II.2: (**a)** Micro-Raman spectra of a wire grown from pyrrole solution (filled circles) and of a polypyrrole film (solid line). (**b)** Micro-Raman spectra of a wire grown from thiophene solution (filled circles) and of a polythiophene film (solid line).

A micro-Raman spectrum for a wire grown from aqueous thiophene-solution is shown in Figure II.2b (filled circles). Also shown is the spectrum of a polythiophene film that was prepared by a standard procedure (solid line)[19,20]. The wire-spectrum agrees with the film-spectrum: both exhibit features at 1240 cm^{-1} (the C-C stretching mode), and 1430 cm^{-1} (the symmetric C═C stretching mode), indicating that this DENA-grown wire is composed of polythiophene.

To characterize the wire-conductivities, we have measured current-voltage (I-V) profiles of polypyrrole and polythiophene electrode-wire-electrode assemblies. After wire-growth, the assemblies were washed with pure water three times and allowed to dry prior to making 2-point I-V measurements with a source-meter (Keithley, 2400). The profiles for 3 polypyrrole wires and 6 polythiophene wires are shown in Figures II.3a and II.3b, respectively. The resistances R of the ~16 μm long polypyrrole wires range from 0.76 to 2.49 MΩ (as given in Table II.1 along with the individual wire-lengths l). The resistances of the longer (~26 μm) polythiophene wires are significantly smaller, ranging from 0.35 to 0.49 MΩ. We approximate the knobby wire-shapes as uniform cylinders with diameters of 560 ± 70 nm for polypyrrole and of 340 ± 70 nm for polythiophene; these are the lengthwise averaged diameter-values, obtained via the electron microscopy-analyses discussed above.

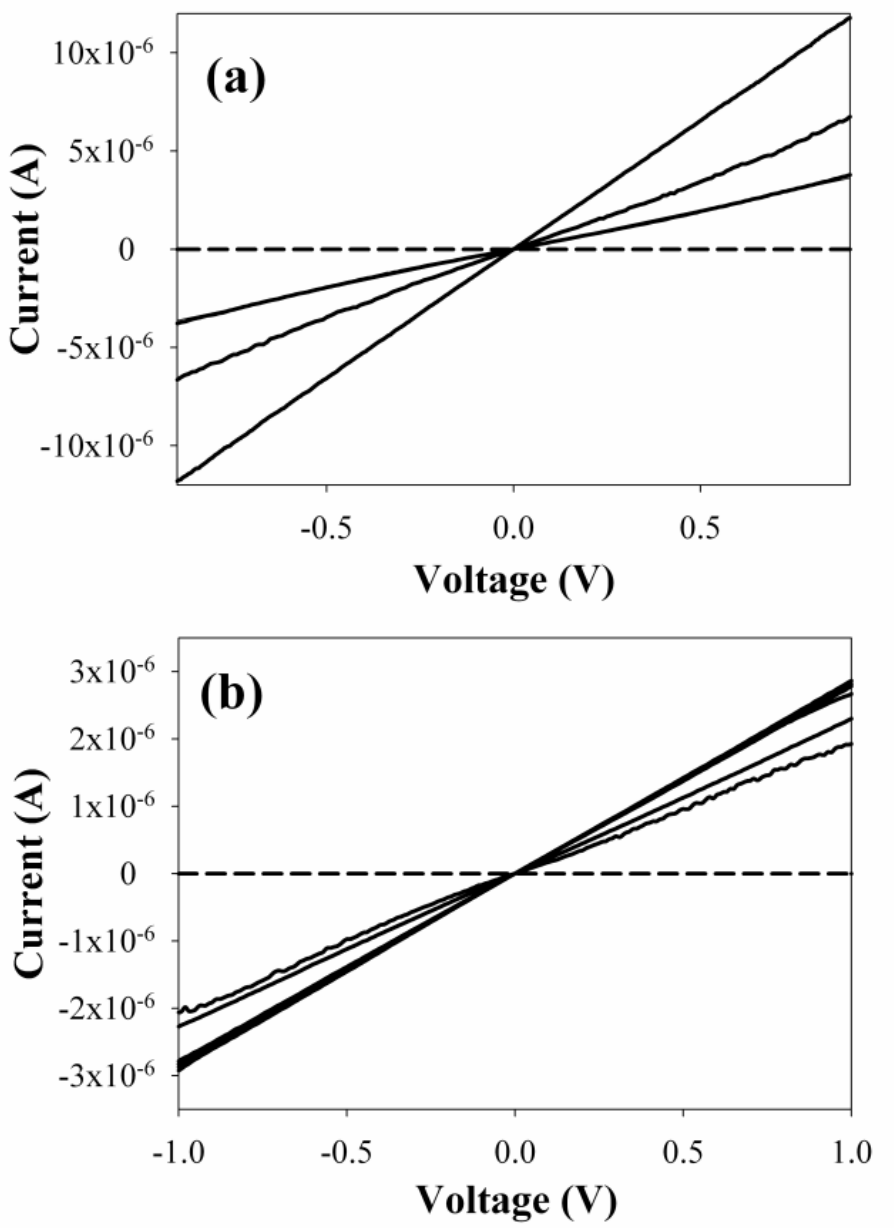

Figure II.3: Current-voltage profiles of electrode-wire-electrode assemblies with (**a)** SDS-doped polypyrrole and (**b)** PSS-doped polythiophene wires. The dashed lines are the I-V profiles of the electrodes (with solution) in the absence of the wires, designating $R > 90\ M\Omega$.

Using the relationship $\sigma = {}^{l}\!/_{RA}$ (where A is the cylindrical cross-sectional area) and the values listed in Table II.1, the conductivities σ of the individual polypyrrole wires were calculated and listed in Table II.1. The average of these 3 determinations is 0.5 ± 0.3 S cm^{-1}, where the uncertainty is the standard deviation of the mean. This value agrees with the previously reported conductivity-value of 0.5 S cm^{-1} for polypyrrole-nanowires.[4] Likewise, the conductivities for the individual polythiophene wires were calculated to give an average value of 7.6 ± 0.8 S cm^{-1} that falls within the established 0.6 to 10 S cm^{-1} range for polythiophene nanowires.[11, 21] Hence, the DENA technique may be used for the single-step fabrication of polymeric electrode-wire-electrode assemblies with conductances that are comparable to those produced by other approaches.

Extending this methodology to enable the fabrication of electrode-wire-target assemblies would provide an innovative way to deliver electrical stimuli to microscopic samples positioned in the inter-electrode gap—a capability of potential electrophysio-logical importance.[22] As the growth-path in the DENA technique is determined by the voltage-profile between the biased and grounded electrode-tips, a critical issue in fabricating such assemblies is whether a dielectric target (such as a cell) perturbs tip-to-tip growth. Thus, Figure II.4a depicts an initial configuration of several *Dictyostelium* cells that are cultured onto an electrode array with one cell in the 30 μm wide electrode-gap. The phosphate buffer needed to maintain the cells contains 10 mM EDOT and 20 mM PSS.[8] Application of a ±3 V, 100 kHz signal to the right electrode induces polythiophene wire-growth. As shown in Figure III.4b, the wire grows essentially along

Polypyrrole	**Length (μm)** (± 0.5 μm)	**Diameter (nm)** (± 70 nm)	**Resistance (MΩ)** (± 0.01 MΩ)	**Conductivity (S cm^{-1})**
Wire 1	16.5	560	0.76	0.88 ± 0.16
Wire 2	16.2	560	1.41	0.47 ± 0.08
Wire 3	16.5	560	2.49	0.27 ± 0.05
Polythiophene				
Wire 1	25.5	340	0.35	8.0 ± 2.4
Wire 2	27.9	340	0.49	6.3 ± 1.8
Wire 3	28.9	340	0.44	7.2 ± 2.1
Wire 4	26.3	340	0.36	8.0 ± 2.4
Wire 5	25.5	340	0.35	8.0 ± 2.4
Wire 6	27.3	340	0.36	8.3 ± 2.4

Table II.1: Parameters for computing the conductivities of the polypyrrole and polythiophene wires.

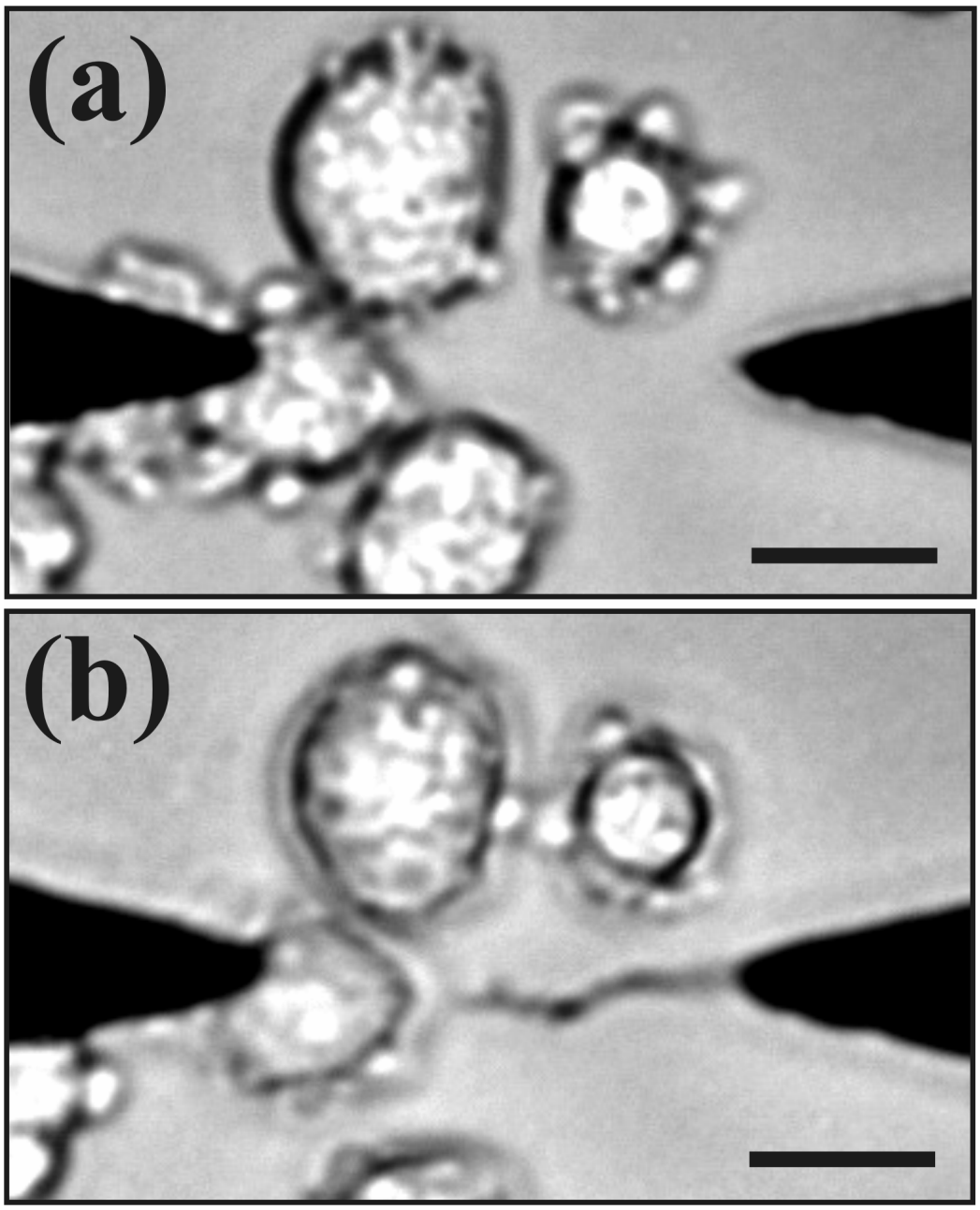

Figure II.4: (a) A configuration of several *Dictyostelium* cells that are cultured onto an electrode array with one cell in the 30 μm wide electrode-gap. (**b)** A polythiophene wire grown from the right electrode up to the live cell that is lying in the gap. The scale bars denote 10 μm.

the line connecting the opposing electrode tips, just as in the cell-free case presented above. By decreasing the voltage-amplitude as the tip approached the cell, the wire was grown to within 1.5 μm of the cell, as depicted in Figure II.4b. Thus, directional growth is still possible even with a dielectric cell in the inter-electrode gap.

This investigation has extended the DENA-technique to enable the template-free growth of conducting polypyrrole and polythiophene wires along predictable growth-paths. This accomplishment enables the fabrication electrode-wire-electrode geometries that are needed for basic transport studies[2, 3] and sensor applications[5, 6] of polymeric wires. This methodology also enables the growth of polymeric wires from on-chip electrodes up to targeted microscopic samples, such as biological cells, that are positioned in the inter-electrode gap. The resulting electrode-wire-target assemblies may find use in physiological applications where electrical signals are routed to user-selected cells for voltage-gated signaling studies. Further work on this application is underway.

II.4 Acknowledgements

This work was supported by grants from the National Science Foundation (research: PHY-646966 and EPS-0447262; instrumentation: DBI-0520678 and EAR-0722410) and the National Institutes of Health (R15 GM073698-01).

REFERENCES

1. C. K. Chiang, C. R. Fincher, Y. W. Park, A. J. Heeger, H. Shirakawa, E. J. Louis, S. C. Gau and A. G. MacDiarmid, Phys. Rev. Lett. **39** (17), 1098-1101 (1977).

2. A. N. Aleshin, H. J. Lee, Y. W. Park and K. Akagi, Phys. Rev. Lett. **93** (19), 196601 (2004).

3. A. Rahman and M. K. Sanyal, Phys. Rev. B **76**, 045110 (2007).

4. S. S. Shiratori, S. Mori and K. Ikezaki, Sensors and Actuators B **49**, 30-33 (1998).

5. N. T. Kemp, D. McGrouther, J. W. Cochrane and R. Newbury, Adv. Mater. **19**, 2634-2638 (2007).

6. Y. Fan, X. Chen, A. D. Trigg, C. Tung, J. Kong and Z. Gao, J. Am. Chem. Soc. **129**, 5437-5443 (2007).

7. S. M. Richardson-Burns, J. L. Hendricks and D. C. Martin, J. Neural Eng. **4**, L6-L13 (2007).

8. S. M. Richardson-Burns, J. L. Hendricks, B. Foster, L. K. Povlich, D. H. Kim and D. C. Martin, Biomaterials **28**, 1539-1552 (2007).

9. K. Ramanathan, M. A. Bangar, M. Yun, W. Chen, N. V. Myung and A. Mulchandani, J. Am. Chem. Soc. **127** (496-497) (2005).

10. M. Woodsen and J. Liu, J. Am. Chem. Soc. **128**, 3760-3763 (2006).

11. A. Das, C. H. Lei, M. Elliot, J. E. Macdonald and M. L. Turner, Organic Electronics **7**, 181-187 (2006).

12. A. Noy, A. E. Miller, J. E. Klare, B. L. Weeks, B. W. Woods and J. J. DeYoreo, Nano Lett. **2** (2), 109-112 (2002).

13. I. Talukdar, B. Ozturk, T. D. Mishima and B. N. Flanders, Appl. Phys. Lett. **88**, 221907 (2006).

14. B. Ozturk, T. Mishima, D. R. Grischkowsky and B. N. Flanders, Nanotechnology **18**, 175707 (2007).

15. B. Ozturk, I. Talukdar and B. N. Flanders, Nanotechnology **18**, 365302 (2007).

16. B. Ozturk, C. Blackledge, D. R. Grischkowsky and B. N. Flanders, Appl. Phys. Lett. **88**, 073108 (2006).

17. A. F. Diaz, J. I. Castillo, J. A. Logan and W. Y. Lee, J. Electroanal. Chem. **129**, 115-132 (1981).

18. J. Mikat, I. Orgzall and H. D. Hocheimer, Phys. Rev. B **65**, 174202 (2002).

19. J. P. McDonald, J. L. Hendricks, V. R. Mistry, D. C. Martin and S. M. Yalisove, J. Appl. Phys. **102**, 013107 (2007).

20. S. Sakamoto, M. Okumura, Z. Zhao and Y. Furakawa, Chem. Phys. Lett. **412**, 395-398 (2005).

21. S. Samitsu, T. Shimomura, K. Ito, M. Fujimori, S. Heike and T. Hashizume, Appl. Phys. Lett. **86**, 233103 (2005).

22. F. Patolsky, B. P. Timko, G. Yu, Y. Fang, A. B. Greytak, G. Zhang and C. M. Lieber, Science **313**, 1100-1104 (2006).

CHAPTER III

Directional growth of metallic and polymeric nanowires

Abstract

This study characterizes an approach called directed electrochemical nanowire assembly for controlling the growth-direction of indium and polythiophene nanowires that are grown electrochemically on micro-electrode arrays. This technique enables nanowire growth from a user selected electrode to within ± 2 μm of a targeted site on a second electrode lying within a ~140 ° angular range and a ~100 μm radius of a selected electrode. A long range component of the applied voltage signal defines the growth-path. Moreover, the presence of this component enables the directional growth of amorphous nanowires, such as polythiophene and polypryrrole.

III.1 Introduction

The technique of *directed electrochemical nanowire assembly* (DENA) enables the template-free, electrochemical growth of metallic nanowires from aqueous salt solutions.[1, 3] In this technique, *the growth-path of the wire is predictable*, as it generally follows the line that connects the foremost tips of a user-selected pair of on-chip electrodes. This behavior is of potential technological importance, as it would provide a single-step approach to interconnecting laboratory instrumentation with sub-microscopic

targets (such as biological cells) to which the wires are grown. A variety of other *single-step* nanowire growth and interconnecting procedures have been developed over the past decade. Dielectrophoretic nanowire-assembly exploits the voltage-induced chaining of metallic nanoparticles into wires that span the gaps between targeted sites on opposing electrodes.[4, 8] A potential drawback of this approach is that these nanoparticulate materials have resistivities several orders of magnitude in excess of bulk metals.[5, 8] Templated growth techniques are in wide-use as they yield reproducible wire-shapes. However, directional growth is only realized by engineering growth-channels before electrochemically depositing the wire.[9, 10] Thus, template-free approaches have been developed for growing conducting polymeric wires[11, 12] between the tips of two electrodes, but the maximum wire-length in these techniques is limited to < 10 μm. Dip-pen lithography relaxes the wire-length constraint and provides excellent control over the positioning of the wires,[13] but is restricted to applications where the use of a scanning probe is feasible. To broaden the range of situations where directional wire-growth is possible, the present work establishes methodology for growing metallic and polymeric wires at user selected sites and across distances as large as 100 μm in on-chip circuitry.

The metallic structures that may be produced by the DENA technique range from needle-shaped wires to highly branched tree-like deposits,[1, 3] two signature structures of the *dendritic solidification* mechanism.[14] (For the wire-growth application, the needle-shaped structures are used). Thus, *dendritic solidification*, a long studied mechanism of diffusion limited growth in the soft condensed matter literature, figures prominently in the DENA-process:[15, 16] It has been established that directional growth is a natural

feature of dendritic solidification. Some background on how this behavior emerges in dendritic solidification is helpful context for the present study, so a brief summary of dendritic solidification theory follows.

In dendritic solidification, the growth velocity v of the dendrite and the radius r of its foremost tip are anti-correlated and dependent on the amplitude of the driving force Δ for the solidification process (*e.g.* applied voltage, supersaturation, or undercooling). This behavior is described by the relation $vr = 2DP(\Delta)$, where the Peclet number $P(\Delta)$ is set by Δ through a formula known as the Ivantsov relation.[17] Thus, the Ivantsov relation permits a continuum of v and r values for a given Δ. Nature, however, is more selective: unique values for v and r are observed for a given Δ, and as a consequence, the dendrite preserves its shape as it grows. Shape preserving growth is somewhat surprising given the reasonable expectation that microscopic deformations of the solidification front will arise due to, say, spatiotemporal fluctuations in the number of solidifying particles on the liquid side of the front. If diffusion to the front were the only important process in its growth, these protrusions would tend to grow at amplified rates because—by virtue of extending farther into the solution—the flux onto the protruding tips would be larger than the flux onto the surrounding depressions. This effect is the Mullins-Sekerka instability,[18] which tends to produce very fine, irregularly branched structures that resemble fractal aggregates.[19, 20, 21, 22] However, if the kinetics of particle-to-surface binding is the rate-limiting step (relative to the organization of the particles to the surface), then the surface tension (or, equivalently, the capillary length d_0) of the solid-liquid interface comes into play. This factor induces the dissolution of protrusions with

small radii of curvature (having large surface-to-volume ratios) in order to minimize the free energy—the Gibbs-Thompson effect.[23] For the deformation mode of precisely the right length scale λ_s, the tendency of the Mullins-Sekerka instability to induce runaway growth is precisely balanced by the tendency of the Gibbs- Thompson effect to induce tip-dissolution. In 1978, dendritic solidification was hypothesized to occur at this marginally stable point; it is a special case where the amplification rate of surface-deformations is exactly zero.[24] Thus, the dendrite grows in a steady, shape-preserving manner. Experimental observations are consistent with this hypothesis as the radius of the dendrite-tip r is found to be of the same scale as the as λ_s, which is reasonable if λ_s is the only mode that grows.[25]

Further insight into this mechanism was attained through the study of the ratio of the stability parameter $\sigma^* = \lambda_s^2/r^2$, a reasonable quantity to examine given that the tip size r is related to the stability length λ_s.[20] As such, σ^* was found to vary with the crystalline anisotropy ε of the solidifying material as $\sigma^* = \sigma_0\varepsilon^{7/4}$. If there is no crystalline anisotropy, dendritic growth is not possible. If there is crystalline anisotropy, then the dendrite grows in the direction that is normal to the crystallographic plane with the largest surface energy. The resulting structures conform with thermodynamic expectations, having large area-sides with small surface energies and small area tips with large surface energies. Moreover, the dependence on crystalline anisotropy reveals *directional growth to be a natural feature of dendritic solidification*.

One would expect, therefore, systems with isotropic surface tension or systems where the surface tension does not play a role in the deposition process, to exhibit random rather than directional growth. Indeed, this expectation is borne out observations of, say, Au adatom diffusion on cold surfaces that yield highly branched Au aggregates with fractal dimensions of 1.7.[19] In contrast, we have recently shown that the DENA technique may be used to grow conducting polypyrrole and polythiophene wires along predictable, inter-electrode paths. Both polypyrrole and polythiophene are amorphous materials with zero crystalline anisotropy. Thus, the natural tendency of these materials is to grow non-directionally, yielding highly ramified, filamentous structures, yet this is not observed. The DENA technique induces these wires grow directionally across 10s-of-microns distances. This observation strongly suggests that the applied voltage underlies the directional growth behavior of the wires.

The present study demonstrates the extent to which the directional-growth of both metallic and polymeric nanowires is attainable with the *DENA* technique. This approach is distinct from most other approaches to achieving directional nanowire growth, as the control is made possible by a long range component of the applied voltage that guides the solidification process between selected electrodes. This control provides a precise means of growing wires in on-chip circuitry from a selected electrode up to a target, which may be a second electrode or an object such as a live cell. Moreover, the presence of this voltage component during the electrochemical polymerization of the amorphous polymeric materials is shown to be necessary in order to realize wire-growth from these materials. Thus, the insight established in this study is expected to enable wire growth

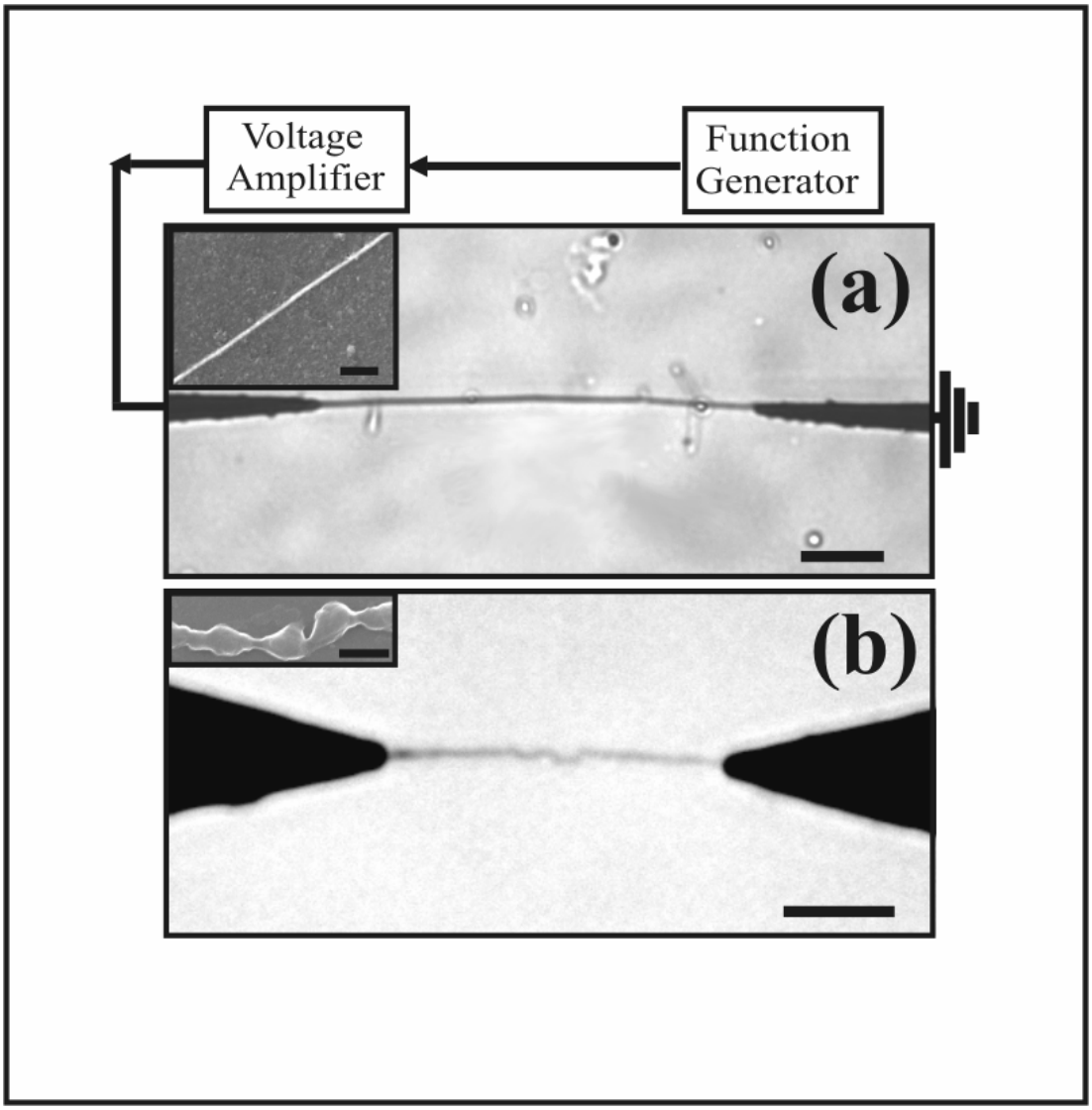

Figure III.2. (a) Apparatus for the directed electrochemical nanowires assembly (DENA) technique. The image is an optical micrograph of an In wire grown along the line connecting the tips of the lithographic electrodes. The scale bar denotes 10 μm. *Inset*. A scanning electron micrograph of an indium nanowire (diameter 106 nm). The scale bar denotes 1 μm. (b) An optical micrograph of a polythiophene wire grown by the DENA technique along the line connecting the tips of the electrodes. The scale bar denotes 10 μm. *Inset*. A scanning electron micrograph of an polythiophene nanowire (diameter 98 nm). The scale bar denotes 100 nm.

from other amorphous materials, such as organic conductors (e.g. TCNQ), ceramics, and biomemitic filaments (actin).

III.2 Experimental Setup

III.21 Indium wire growth

The experimental apparatus for the DENA technique is shown in figure III.1(a), consisting of sharp, transiently biased electrodes immersed in concentrated salt solution. This apparatus is described in detail elsewhere.[1] Briefly, the optical micrograph in this figure depicts an indium nanowire spanning the 60 μm gap between the ends of a tapered electrode pair. The electrodes were deposited in 12-pair arrays on quartz substrates using standard lithographic techniques[8] and are composed of 100 nm thick base layers of Ti and 500 nm thick top-layers of Al. The wire shown in this micrograph was grown by depositing a 10 μl aliquot of aqueous 0.055 M $In(CH_3COO)_3$ solution across the electrodes and applying an ±18 V square-wave with a 50 % duty cycle to the left electrode while the right electrode was grounded. Growth does not occur when voltage amplitudes less than 18 V are used. A *square* waveform is optimal, as sinusoidal or sawtooth waveforms require larger voltage-amplitudes to induce growth (> 40 V). Presumably, square-waves are more effective because they apply the full voltage for (nearly) the entire half-period, whereas a sine wave reaches the full amplitude for only an instant during its half-cycle. Additionally, duty cycles not equal to 50 % result in rapid electrode-dissolution, thereby preventing wire-growth. The frequency ω of the alternating voltage may be varied between 0.5 MHz and 3.5 MHz for In wire-growth. As

explained elsewhere, this degree-of-freedom provides sensitive control over the wire-diameter and growth velocity.[3]

III.22 Polythiophene wire growth

Wires may be grown from several other materials, as well (*metals:* Co, Ni, Pd,[26] Pt, Ag, Au, Zn, and Pb; *conducting polymers:* polythiophene and polypyrrole[27]). Figure III.1a depicts the apparatus for growing conducting polythiophene nanowires between the electrodes, which were prepared as described above for *Indium wire growth*.[8] This wire was grown by depositing 10 μl of aqueous solution containing 0.01 M ethylenedioxy-thiophene (EDOT) and 0.02 M poly(sodium styrene sulfonate) (PSS) across the electrodes. A voltage-signal with an amplitude of ± 2.5 V and a frequency of 100 kHz was used to induce wire-growth across the 30.2 μm gap in Figure III.1b. The inset depicts a scanning electron micrograph of the wire. Its structure is knobby, varying from 98 to 669 nm in thickness with a lengthwise averaged diameter of 340 nm.

III.3 Theory

The growth-path of the wires is well-described by the straight line that connects the tips of the alternating and grounded electrodes—even for polymeric wires having no crystalline anisotropy. This behavior suggests that the applied voltage defines the growth-path coinciding with the line of electric field maxima that extends from the biased electrode tip through the solution and to the grounded electrode. A voltage-profile corresponding to a uniform electric field ($-V_{app}/L$) in the inter-electrode gap is denoted by

the solid line in Figure III.3. However, because medium between the electrodes is electrolytic, ions near the biased electrode will respond in a Coulombic manner to the applied voltage and, thereby, rearrange to screen the voltage over a short (< 10 nm) distance. This is analogous to the Debye-Hückel effect,[28] and the screening distance λ_D is ~ 1 nm for a 55 mM electrolyte, such as aqueous $In(CH_3COO)_3$.[29] A voltage profile corresponding complete screening of the field across a short distance relative to the gap-length is illustrated by the dashed line in Figure III.3. The major treatises on electrochemistry indicate that the applied voltage is only partially screened, enabling a significant long-range component to extend across the entire electrode gap.[28] Thus, it is the combination of the processes associated with the voltage profiles in Figure III.3 that must be considered. It has been our experience that insight into how this process emerges from the governing diffusion equations is difficult to extract from these sources. Therefore, to compactly present the theoretical origin of this phenomenon and to relate this theory to the precise directional growth attainable in the DENA technique, the spatial dependences of the ionic concentrations and the electric potential in a 1D inter-electrode region is described below.

To analyze this directional growth behavior, we consider the one-dimensional motion of ions in solution in response to externally applied electric fields, as well as the field that arises due to the organization of the charges within the solution. Further we assume the body forces on the solution are sufficiently small that convection is negligible: we need not include hydrodynamics. At this level, we consider continuity equations for each of the charged species. For simplicity we assume a single positive and

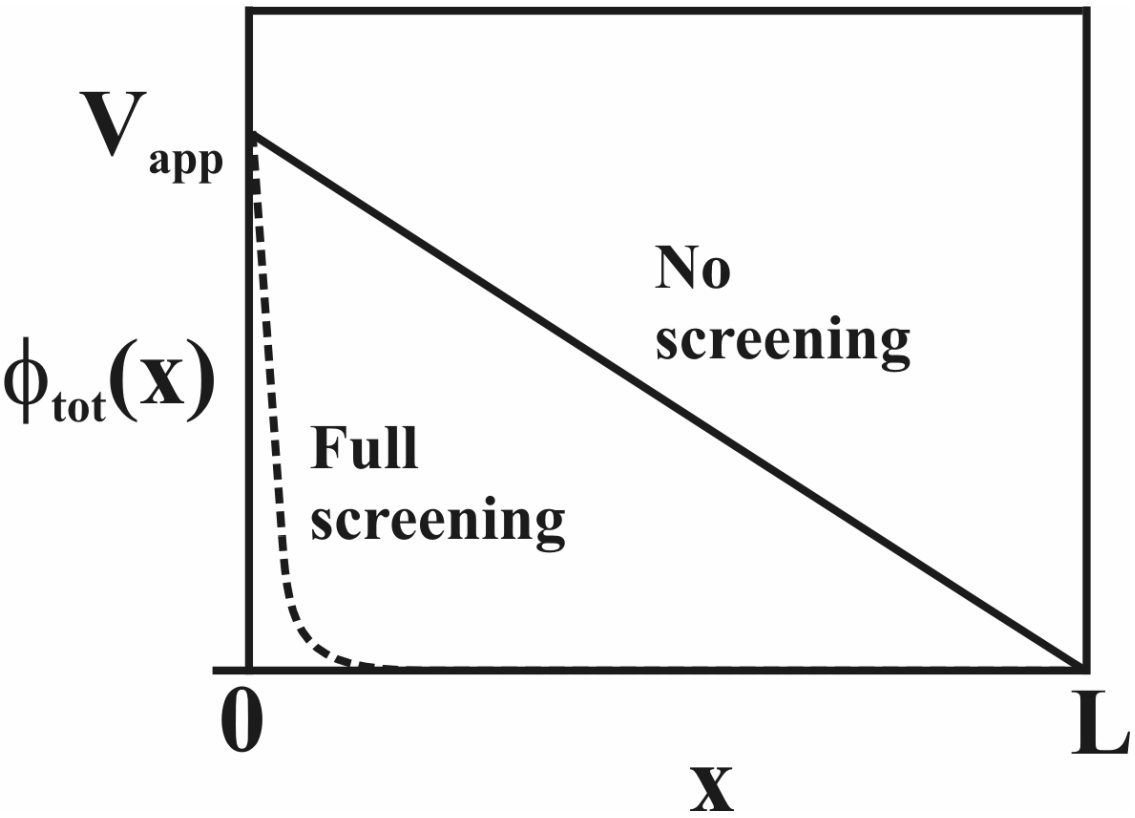

Figure III.3. Potential profiles $\phi(x)$ for the cases of no screening (solid line) and full screening (dashed line) of a voltage V_{app} that is applied to the left wall of the cell. The right wall is grounded.

single negative species. Hence the two continuity equations (conservation of species-type) are as follows:

$$\partial_t C_1(x,t) = -\nabla \cdot \vec{j}_1(x,t) \tag{III.1a}$$

and

$$\partial_t C_2(x,t) = -\nabla \cdot \vec{j}_2(x,t). \tag{III.1b}$$

Here $C_1(x, t)$ and $C_2(x, t)$ are the spatially dependent concentrations of the positive and negative ions, respectively, and $j_1(x, t)$ and $j_2(x, t)$ are the corresponding local fluxes of these species. The fluxes may be written in terms of concentration gradients $\nabla C_i(x, t)$ and electric forces $-z_i e \nabla\phi(x, t)$ acting on the species, where $\phi(x, t)$ is the electric potential and z_i is the valence of species i:

$$j_1 = -D_1 \nabla C_1 - \beta D_1 z_1 e \nabla \phi C_1 \tag{III.2a}$$

and

$$j_2 = -D_2 \nabla C_2 + \beta D_2 z_2 e \nabla \phi C_2 \tag{III.2b}$$

D_1 and D_2 are the diffusion constants of the cationic and anionic species, respectively, and e is $1.602*10^{-19}$ C. For the sake of brevity, the spatial and temporal dependences of the quantities j_i, C_i, and ϕ will be taken to be implicit for the remainder of this section.

Let the potential ϕ is comprised of two parts: ϕ_{Sol} arising from net charge concentrations within the solution and ϕ_{Drift} representing the unscreened portion of the externally applied voltage. The Poisson equation

$$\nabla^2\phi_{Sol} = -\frac{e}{\varepsilon\varepsilon_0}\left(z_1C_1 - z_2C_2\right) \tag{III.3a}$$

must be satisfied in the case of potentials produced by net charge within the solution, whereas the Laplace equation

$$\nabla^2\phi_{Drift} = 0 \tag{III.3b}$$

is satisfied in the case of externally applied fields. The total potential is the sum of the two:

$$\phi(x,t) = \phi_{Sol}(x,t) + \phi_{Drift}(x,t). \tag{III.4}$$

Here we linearize the equations of motion. Let $C_1 = C_{0,1} + \delta C_1$ and $C_2 = C_{0,2} + \delta C_2$ where $C_{0,1}$ and $C_{0,2}$ are the bulk concentrations for species 1 and 2; net neutrality is imposed by the condition $z_1C_1 - z_2C_2 = 0$. Substituting these concentration expressions into equations (III.2a) and (III.2b), allows equations (III.1a) and (III.1b) to be re-written as follows:

$$\partial_t\left(C_{0,1} + \delta C_1\right) = D_1\nabla^2\left(C_{0,1} + \delta C_1\right) + \beta D_1\nabla\cdot\left(z_1e\nabla\phi\left(C_{0,1} + \delta C_1\right)\right) \tag{III.5a}$$

and

$$\partial_t\left(C_{0,2}+\delta C_2\right)=D_2\nabla^2\left(C_{0,2}+\delta C_2\right)-\beta D_2\nabla\cdot\left(z_2e\nabla\phi\left(C_{0,2}+\delta C_2\right)\right). \qquad \text{(III.5b)}$$

The effects of the two voltage components, ϕ_{Sol} and ϕ_{Drift}, on the ionic concentrations are introduced into this description by invoking equation (III.4). Equations (III.5a) and (III.5b) are, thus, expanded to

$$\begin{aligned}\partial_t\delta C_1 = {} & D\nabla^2\delta C_1+\beta Dz_1e\nabla^2\phi_{Sol}C_{0,1}+\beta Dz_1e\nabla\phi_{Drift}\cdot\nabla\delta C_1 \\ & +\beta Dz_1e\nabla^2\phi_{Sol}\delta C_1+\beta Dz_1e\nabla\phi_{Sol}\cdot\nabla\delta C_1\end{aligned} \qquad \text{(III.6a)}$$

and

$$\begin{aligned}\partial_t\delta C_2 = {} & D\nabla^2\delta C_2-\beta Dz_2e\nabla^2\phi_{Sol}C_{0,2}-\beta Dz_2e\nabla\phi_{Drift}\cdot\nabla\delta C_2 \\ & -\beta Dz_2e\nabla^2\phi_{Sol}\delta C_2-\beta Dz_2e\nabla\phi_{Sol}\cdot\nabla\delta C_2\end{aligned}. \qquad \text{(III.6b)}$$

where we have let $D_1 = D_2 = D$. To expedite the solution of these differential equations below, we make the simplification that $z_1 = z_2 = z$ (*i.e.* both species have the same valence), which implies by the charge neutrality condition that $C_{0,1} = C_{0,2} = C_0$. By noting that equation (III.3a) may be re-written as $\nabla^2\phi_{Sol} = -e\varepsilon^{-1}(\delta C_1 - \delta C_2)$, equations (III.6a) and (III.6b) reduce to

$$\partial_t\delta C_1\cong D\nabla^2\delta C_1-\frac{\beta Dz^2e^2}{\varepsilon\varepsilon_0}\left(\delta C_1-\delta C_2\right)C_0+\beta Dze\nabla\phi_{Drift}\cdot\nabla\delta C_1 \qquad \text{(III.7a)}$$

and

$$\partial_t\delta C_2\cong D\nabla^2\delta C_2+\frac{\beta Dz^2e^2}{\varepsilon\varepsilon_0}\left(\delta C_1-\delta C_2\right)C_0-\beta Dze\nabla\phi_{Drift}\cdot\nabla\delta C_2 \qquad \text{(III.7b)}$$

where only the terms up to first order in δC_1 and δC_2 were kept.

This set of coupled differential equations may be further simplified by adding and subtracting them and then making steady-state approximations ($\partial_t \delta C_i = 0$) to obtain

$$0 = D\nabla^2\psi + \beta DeE_{Drift}\nabla\rho \tag{III.8a}$$

and

$$0 = D\nabla^2\rho - \kappa^2\rho + \beta DeE_{Drift}\nabla\psi \tag{III.8b}$$

where $\psi = \delta C_1 + \delta C_2$, $\rho = \delta C_1 - \delta C_2$, and $\kappa^2 = 2\beta Dz^2e^2C_0/\varepsilon$.

These equations are second-order, inhomogeneous differential equations, suggesting solutions of the exponential form $e^{\lambda x}$ for both ρ and ψ.[30] Following the substitution of this form into Equations (III.8a) and (III.8b), simultaneous solution of the resulting equations yields the allowed set of λ-values:

$$\lambda = \beta e\frac{V}{L}\sqrt{1+2\frac{L^2C_0}{\beta\varepsilon\varepsilon_0V^2}}\ . \tag{III.9}$$

Thus, we have the following general solutions for ρ and ψ:

$$\rho = A_1e^{-\lambda x} + A_2e^{\lambda x} \tag{III.10a}$$

and

$$\psi = B_1e^{-\lambda x} + B_2e^{\lambda x}\ , \tag{III.10b}$$

where A_1, A_2, B_1, and B_2 are integration coefficients that will be determined below. From these results, the following results for the concentration profiles C_1 and C_2 are derived:

$$C_1 = C_0 + \tfrac{1}{2}(A_1 + B_1)e^{-\lambda x} + \tfrac{1}{2}(A_2 + B_2)e^{\lambda x} \qquad \text{(III.11a)}$$

and

$$C_2 = C_0 + \tfrac{1}{2}(B_1 - A_1)e^{-\lambda x} + \tfrac{1}{2}(B_2 - A_2)e^{\lambda x} \qquad \text{(III.11b)}$$

With knowledge of C_1 and C_2, the potential ϕ, consisting of components ϕ_{Sol} and ϕ_{Drift}, may now be further described. Let $\phi(0) = V_{App}$ be the total potential that is applied to the left wall (electrode) in Figure III.2. Therefore,

$$V_{App} = \phi_{Drift}(0) + \phi_{Sol}(0) \qquad \text{(III.12a)}$$

$\phi_{Drift}(0)$ differs from V_0 when there is steady state screening of the electrode that is described by the first order terms in equations (III.7a) and (III.b). Furthermore, we assume that the drift field $E_{Drift} = -\nabla\phi_{Drift}$ is uniform, so the flux that it drives is divergence-less: $\nabla \cdot J = -\beta DeC_o \nabla \cdot E_{Drift} = 0$. It follows that the constant concentrations in a constant field represent a current flux through the sample. Hence, ϕ_{Drift} is expressed as

$$\phi_{Drift}(x) = -E_{Drift}(L - x) \qquad \text{(III.12b)}$$

where we have used the fact that the grounded electrode at $x = L$ has zero potential. The screening potential $\phi_{Sol}(x)$ may be determined by direct integration,

$$\phi_{Sol}(x) = -\int \left(\int \frac{e}{\varepsilon}(C_1 - C_2)dx_{pp} \right) dx_p \,, \tag{III.12c}$$

which is another form of the Poisson equation (equation (3b)). Substitution of Eqns. (III.11a) and (III.11b) and the assumption that $\delta C_1 = -\delta C_2$ enables the straight-forward integration of Eqn. (III.12c), yielding

$$\phi_{Sol}(x) = -\frac{e\left(A_1 e^{-\lambda x} + A_2 e^{\lambda x}\right)}{\varepsilon \lambda^2} \,. \tag{III.13}$$

Application of the boundary conditions $\phi_{Sol}(0) = \phi_{Sol,0}$ (which is yet to be determined) and $\delta\phi_{Sol}(L) = 0$ yields the integration constants A_1 and B_2:

$$A_1 = -\frac{\varepsilon \lambda^2 \delta\phi_{Sol,0} e^{\lambda L}}{e\left(e^{\lambda L} - e^{-\lambda L}\right)} \tag{III.14a}$$

and

$$A_2 = -\frac{\varepsilon \lambda^2 \delta\phi_{Sol,0} e^{-\lambda L}}{e\left(e^{\lambda L} - e^{-\lambda L}\right)} \,. \tag{III.14b}$$

With these results, for A_1 and A_2, equations (III.11a) and (III.11b) for the concentration profiles, C_1 and C_2 are now determined. These profiles are plotted in Figure III.3(a), where C_1 (solid line) and C_2 (dashed line) are seen to deviate from the bulk concentration of 55 mM only near the negatively biased right wall. For clarity, an unrealistically large value of λ^{-1} was used in this plot, so the screening length in Figure III.3(a) is of the order of 300 nm, not ~1 nm, as expected of a 55 mM salt solution. The other parameters are given in the accompanying caption.

Likewise, the voltage profiles $\phi_{Drift}(x)$ and $\phi_{Sol}(x)$ given by equations (III.12b) and (III.13) are also solved:

$$\phi_{Drift}(x) = -E_{Drift}(L-x) \tag{III.15a}$$

and

$$\phi_{Sol}(x) = -\phi_{Sol,0}\frac{\sinh[\lambda(L-x)]}{\sinh[\lambda L]} \tag{III.15b}$$

Substituting equations (III.15a) and (III.15b) into equation (III.4) yields the position dependent voltage profile:

$$\phi(x) = -\left(E_{Drift}(L-x) + \phi_{Sol,0}\frac{\sinh[\lambda(L-x)]}{\sinh[\lambda L]}\right) \tag{III.16}$$

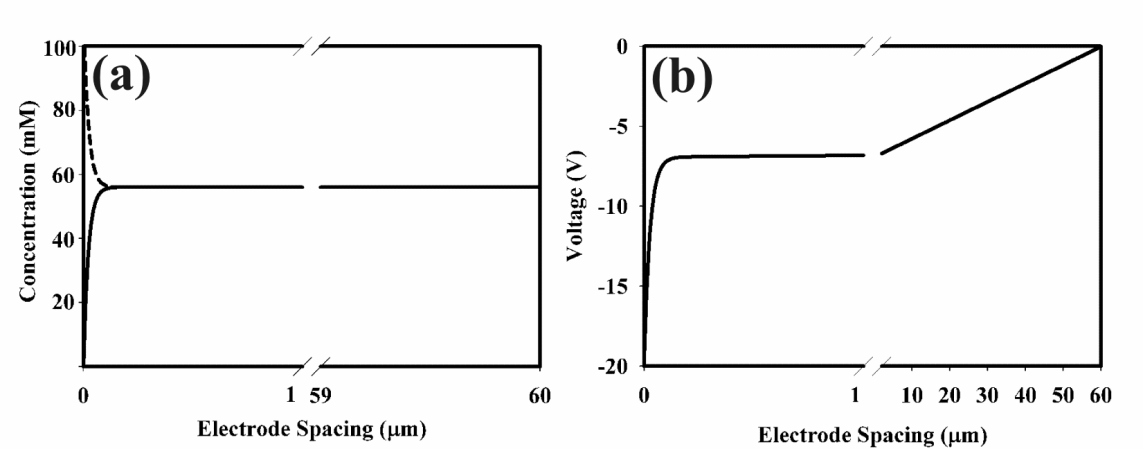

Figure III.4. (a) The concentration profiles for C_1 (solid line) and C_2 (dashed line) that were calculated via equations (III.11a) and (III.11b), respectively. An over-large large value of λ equal to 2283 μm^{-1} used to calculate these profiles. (b) The voltage profile in the solution, calculated via equation (16). For this plot, V_{app} = -20 V and $\phi_{Sol,0}$ = -12 V. The value of λ that was used in panel (a) was used here.

Equation (III.16) is the primary result of this analysis. This equation indicates that the potential at any point x in the solution is composed of two components, one of initial magnitude $\phi_{Sol,0}$ that is screened out across a length scale of λ^{-1}, and one of initial magnitude $E_{Drift}L$ that decays across the entire gap-length L. An example of such a partially screened voltage profile is plotted in Figure III.3(b), using the same screening and gap-lengths as were used for Figure III.3(a). Depending on the magnitude of $E_{Drift}L$, a significant fraction of the applied voltage may extend across the entire gap-length.

III.4 Results

Figures III.1(a) and (b) show that the DENA technique causes both metallic and polymeric wires to grow along the line bridging the biased and grounded electrode tips. The wire composed of crystalline indium, which has non-zero crystalline anisotropy, may owe the directional character of its growth to either its crystalline anisotropy or to the external voltage. However, the wire composed of amorphous polythiophene has no crystalline anisotropy, yet it still exhibits directional growth. This behavior indicates that the directional character of the DENA technique is due to the externally applied voltage.

The theoretical analysis presented above indicates that when the applied voltage is only partially, rather than fully, screened, a voltage component that is a significant fraction of the applied voltage, extends entirely across the gap to the grounded electrode. To assess the extent to which this component arises in practice, equation (III.16) must be evaluated using realistic values for the parameters $\phi_{Sol,0}$ and $E_{Drift}L$. To do this, we

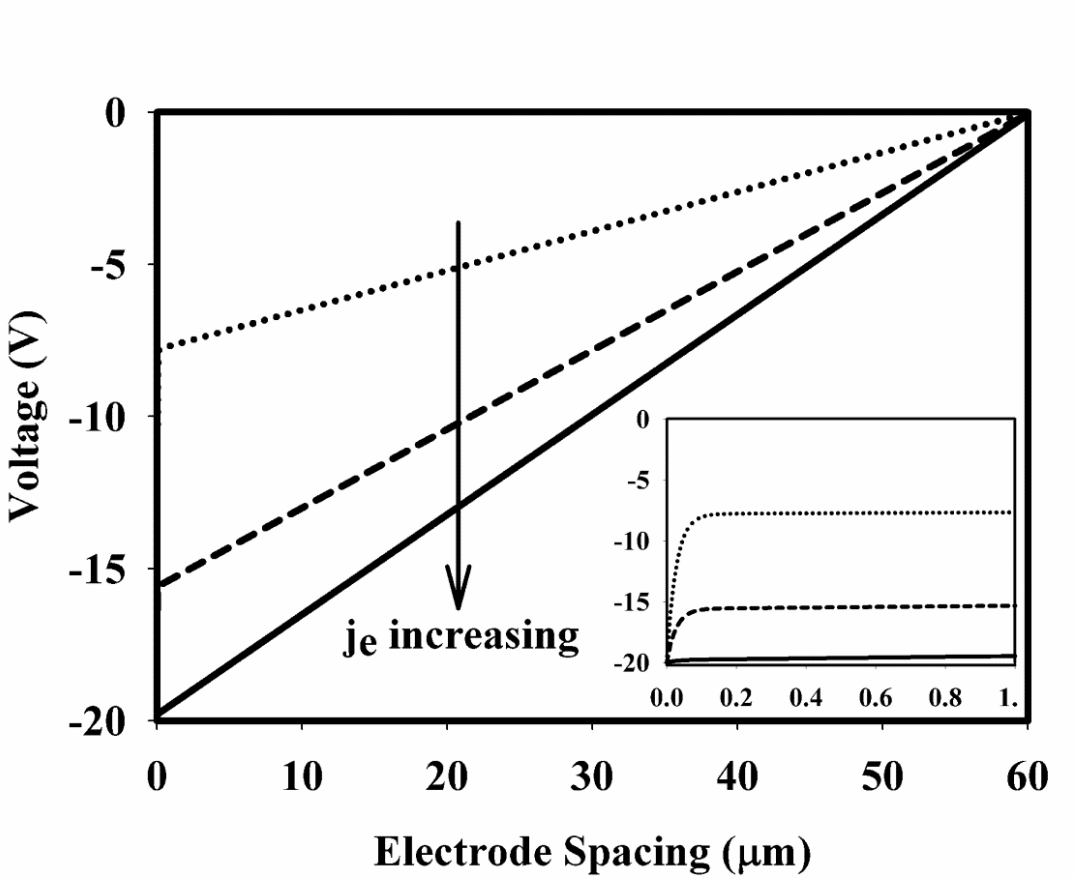

Figure III.5. The voltage profiles in the solution, calculated via equation (III.16). The different profiles correspond to different values of j_e, which sets the parameter $\phi_{Sol,0}$, with j_e increasing in the direction indicated by the arrow.

assume that growth occurs when the system is in a steady state, so the cationic flux is uniform across the system. Hence, the flux j_e at the electrode-electrolyte interface $j_1(0) = j_e$ must equal the flux elsewhere in the solution j_{Drift}. The deposition that is responsible for wire-growth occurs at the interface; this flux is given by the mass conservation boundary condition: $j_e = v(\rho - c_{int})$,[3] where v is the (observable) growth velocity of the wire, and ρ is the (number) density of the wire-material. For an indium wire grown with an applied voltage of $V_{App} = \pm 20$ V , $\rho_{In} = 3.8 \times 10^{10}$ μm^{-3}, and a typical value for the growth velocity is 26 μm s^{-1}, j_e is found to be 9.9×10^{11} μm^{-2} s^{-1} [3]. Invoking the steady-state condition and the relationship $j_{Drift} = \beta DzeE_{Drift}C_0$, the parameter $E_{Drift}L$, which sets the size of the long range potential in equation (III.16), is determined to be $E_{Drift}L = j_eL/(\beta DzeC_0)$. Using $\beta = 2.44 \times 10^8$ kg^{-1} μm^{-2} s^2 C (for $T = 300$ K), $D = 1000$ μm^2 s^{-1}, $z = 3$, $L = 60$ μm, and $C_0 = 55$ mM $= 3.31 \times 10^7$ μm^{-3} (which are the parameters used elsewhere{Ozturk, 2007 #1020}), $E_{Drift}L$ is computed to be -15 V. Thus, a voltage equal to 75 % of V_{App} drops linearly across the gap. The corresponding parameter $\phi_{Sol,0}$ is -5 V, as determined by equation (III.16) evaluated at $x = 0$. The dashed curve in Figure III.4 denotes the full voltage profile (*i.e.* equation (III.16)) that corresponds to these parameters. As another example, the profile corresponding to a growth velocity of 13 μm s^{-1} has a drift magnitude $E_{Drift}L$ = -7.6 V and a screening magnitude equal to -12.4 V. This profile is shown as a dotted line in Figure III.4. Thus, we see that for realistic sets of experimental parameters, a significant fraction of V_{app} is not screened but instead extends across the entire electrode gap.

While the straight-line growth of Figures III.1(a) and III.1(b) depict wire-growth to the only other object in the system, findings that are consistent with the notion that a long range voltage component defines the growth path, a more demanding probe of this behavior would be to study how the wire-grows when there are several objects available to grow towards; which path does the wire choose? The electrode array in Figure III.5(a) illustrates the experimental layout that we have designed to characterize this situation. The optical micrograph depicts a 16-electrode array, where the spacing between the tips of the electrodes in this array varies from 20 μm for a neighboring pair to over 100 μm for two electrodes on opposite sides of the array. Indium wires were grown in this study, as described above. A different electrode was grounded in each of the six trials depicted in Figures III.5 (a)-(f), whereas the same electrode was biased with the growth initiating voltage signal. (When numbered counter-clockwise, starting from the uppermost electrode on the left side, the biased electrode is electrode 2). Nothing was done to any of the other 14 electrodes. During growth, the drop of solution encompassed all of the electrodes. In the situation depicted in figure 5(a), for example, we find that even though electrodes 1 and 3 were closer to electrode 2, where growth initiated, the wire grew to electrode 16; the wire did not simply grow to the nearest metallic object. The same behavior was observed in the situations depicted in Figures III.5(b)-(f). The tip-to-tip distances for these electrode pairs vary from 41.2 μm for pair 2-16 to 94.3 μm for pair 2-11. With reference to the horizontal line connecting electrodes 2 and 11, the path-angle varies from +65° for pair 2-16 to -72 ° for pair 2-5, demonstrating directional control across a 137° range. In each of these cases, the growth path lies within ± 2 μm of the straight line connecting the selected pair of electrode tips.

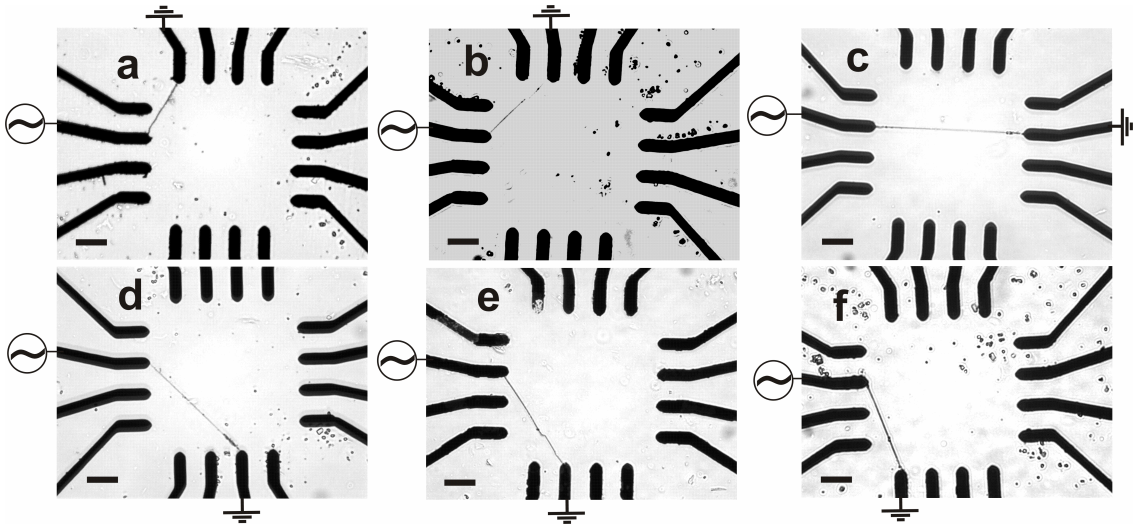

Figure III.5: A series of nanowires that have been grown between user-selected electrode pairs where the alternating and grounded electrodes are electrodes (a) 2 and 16, (b) 2 and 15, (c) 2 and 11, (d) 2 and 7, (e) 2 and 6, and (f) 2 and 5, respectively, where the electrodes are numbered counter-clockwise, starting from the uppermost electrode on the left-hand side. The scale bars denote 20 μm.

In fact, the wire in Figure III.5(e), which grew from electrode 2 to electrode 7, has a step that is positioned about 2/3 of the way along its length; thus, the wire undergoes a correction in its growth path that places it in closer register with the straight inter-electrode line. These results shows that the user may specify the growth path by selection of the biased and grounded electrodes, as the wire grows along the shortest path between the tips of these electrodes.

A numerical description of the 16 electrode array shown in Figures III.5(a)-(f) is relatively straight-forward. Hence, we have employed a finite element analysis routine (FemLab) to calculate the electric potential and the current density in the inter-electrode region of such an array of conductors. In this analysis, a steady voltage is applied to one electrode, while another is grounded; nothing is done to the remaining 14 conducting electrodes. The aim is to characterize the long range component of the applied voltage in the inter-electrode region, so screening is not included (*i.e.* the inter-electrode medium is described simply by a uniform dielectric constant). Figure III.6(a) depicts the optical micrograph of an indium wire grown from electrode 2 to electrode 7, as described above. Figure III.6(b) depicts the finite element analysis-results for this situation. The equipotential profiles are shown in color and indicate that the voltage increases across the gap from -10 V at electrode 2 to 0 V at electrode 7. Near the electrodes, these contours reflect the electrode-geometries, but closer to the middle of the gap, the contours are relatively straight. As the electric field at a given point is perpendicular to the equipotential profile at that point and is directed towards the negatively biased electrode,

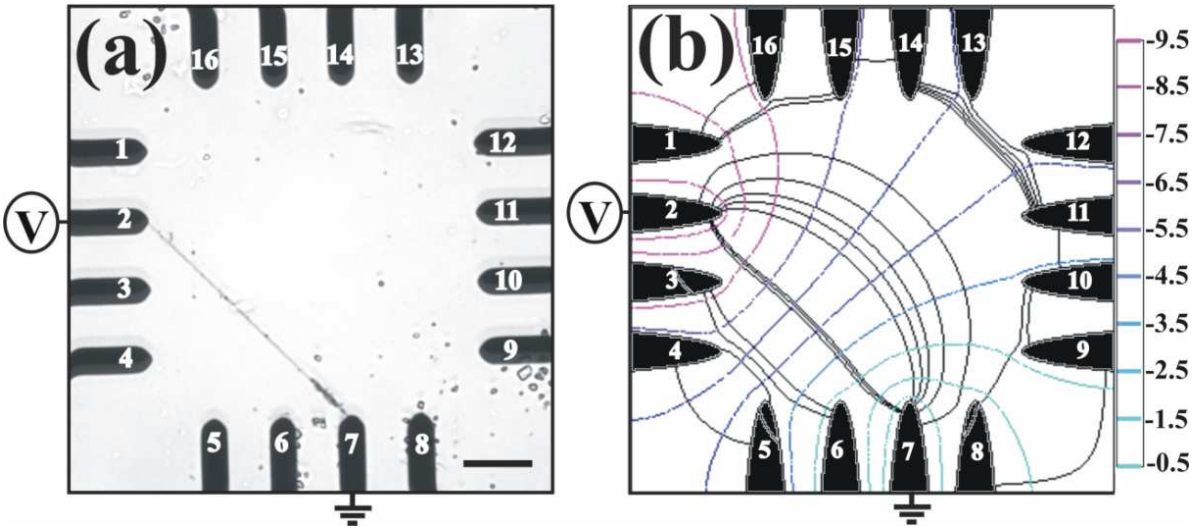

Figure III.6. (a) Optical micrograph of a wire grown from electrode 2 to electrode 7 (identical to Figure III.6(d)). The scale bar denotes 20 μm. (b) A numerically calculated two dimensional map of the electric potential (colored contours) and current density (black contours) on a 16 electrode array when electrode 2 is biased and electrode 7 is grounded.

these profiles describe a field vector that extends in essentially a straight line from the tip of electrode 7 to the tip of electrode 2. This field drives a current-density of positive charge along this line, towards electrode 2, as indicated by the black equi-current contours in the figure. Thus, this analysis predicts that wire growth will occur along the vector describing the ridge of electric field maxima in the inter-electrode region because the cationic flux that feeds the growing wire is maximized along this vector. Indeed, the position of the wire in Figure III.6(a) is well described by this predicted pathway in Figure III.6(b).

III.5 Discussion

The central hypothesis of this study is that the directional character of the DENA technique is due to the externally applied voltage. This work is motivated by a recent study which found that DENA is effective at growing nanowires from amorphous materials (conducting polymers) that have no crystalline anisotropy.[27] The one dimensional diffusive model that was analyzed in this study supports this hypothesis. That is, for realistic experimental parameters (i.e. those actually used in DENA-based indium wire growth), the fraction of V_{app} that is not screened but instead extends across the entire electrode gap is calculated to vary from 5% to 80 % (see Figure III.4). Furthermore, numerical analysis of more complex electrode geometries (the 16 electrode array), in which the long range voltage-component is the only voltage source included in the model, successfully predict the experimentally observed path of nanowire growth. In light of these analytical results, we conclude a critical condition for realizing directional

control in DENA technique is the existence of a significant long-range voltage component that extends across the electrochemical cell.

The physical picture that emerges from this analysis is that *complete* screening (see the dashed profile in Figure III.3) must not occur if long range directional growth is to be realized in the DENA technique. An alternating voltage is used to induce growth in this approach. During each half cycle, the electrolytic system evolves towards the steady state $j_{Drift} = j_e$ where the flux of the electroactive species is uniform across the cell. The screening layer evolves during the time before the steady-state is attained. The rate at which particles flow into the screening layer is given by the drift flux j_{Drift}, and the rate at which particles are removed from the screening layer is dictated by the electrode flux j_e. The screening layer builds up so long as $j_{Drift} > j_e$ because electrode cannot accept (oxidize or reduce) all of the particles that flow to the electrode-electrolyte interface. (The particle-to-surface attachment kinetics determines j_e, but a detailed consideration of this factor lies beyond the scope of this work.)[31] However, j_{Drift} evolves in lockstep with the screening layer, because as ions build up around the electrode, they screen the applied field. As a result, the field in the bulk of the solution (beyond the screening layer) decreases in magnitude. The steady state is thereby attained when the flux across the gap is uniform: $j_{Drift} = j_e$. So long as j_e is finite, j_{Drift} and, hence, E_{Drift} will be non-zero.

This physical picture also illustrates the mechanism by which the wire grows. Figures III.5 (a)-(f) illustrate that the user may specify the nanowire growth path in the DENA technique by selection of biased and grounded electrodes, as the wire grows

along the shortest path between the tips of these electrodes. The finite element analysis-based results of this system indicate that a ridge of electric field maxima extend between the two selected electrodes. By Ohms law, the current-density of positive charge is maximized along this line. Thus, the growth path coincides with this line because the flux of particles that feeds the growing wire is maximized along this vector. For indium wires, these particles are indium cations, whereas they are the sulfate counter-ions in conducting polythiophene wire growth. We see that it is the current of particles that defines the growth path, and therefore, factors that will disrupt this current will destroy the directional control. Figure 4 estimates of ϕ_{Drift} for indium wire growth to range from 6 V to 19 V. The ratio of the potential energy of an In^{3+} cation in ϕ_{Drift} to the thermal energy at 300 K ranges from 600-2000, so the values of ϕ_{Drift} that are realized experimentally are sufficient to overcome the randomizing forces of thermal energy.

III.6 Conclusion

This work has shown the DENA technique is capable of inducing nanowire growth along user-specified paths in on-chip circuitry that originate in a long range component of the applied voltage. As such, growth occurs along the path of E-field maxima that extends from the biased to grounded electrodes because the drift flux j_{Drift} is largest along this path. Hence, the solidification front is advances through the solution at its fastest rate along this path. This finding is significant because it would not be possible to electrochemically fabricate polymeric nanowires in a template-free manner without this effect. As will be delineated in later chapters, the ability to grow flexible polymeric

wires enables an innovative means of probing the forces exerted by migrating *Dictyostelium* cells.

III.7 Acknowledgements.

This work was supported by the National Science Foundation (PHY-646966) and Oklahoma EPSCoR (EPS-132354).

REFERENCES

[1] Talukdar I, Ozturk B, Mishima T D and Flanders B N 2006 Directed growth of single crystal indium wires *Appl. Phys. Lett.* **88** 221907

[2] Ozturk B, Mishima T, Grischkowsky D R and Flanders B N 2007 Single step growth and low resistance interconnecting of gold nanowires *Nanotechnology* **18** 175707

[3] Ozturk B, Talukdar I and Flanders B N 2007 Directed growth of diameter-tunable nanowires *Nanotechnology* **18** 365302

[4] Bezryadin A, Westervelt R M and Tinkham M 1999 Self-assembled chains of graphitized carbon nanoparticles *Appl. Phys. Lett.* **74** 2699-701

[5] Hermanson K D, Lumsdon S O, Williams J P, Kaler E W and Velev O D 2001 Dielectrophoretic assembly of electrically functional microwires from nanoparticle suspensions *Science* **294** 1082-6

[6] Kretschmer R and Fritzsche W 2004 Pearl chain formation of nanoparticles in microelectrode gaps by dielectrophoresis *Langmuir* **20** 11797-801

[7] Ozturk B, Talukdar I and Flanders B N 2005 The directed-assembly of CdS interconnects between targeted points in a circuit *Appl. Phys. Lett.* **86** 183105

[8] Ozturk B, Blackledge C, Grischkowsky D R and Flanders B N 2006 Reproducible interconnects assembled from gold nanorods *Appl. Phys. Lett.* **88** 073108

[9] Ramanathan K, Bangar M A, Yun M, Chen W, Myung N V and Mulchandani A 2005 Bioaffinity sensing using biologically functionalized conducting-polymer nanowire *J. Am. Chem. Soc.* **127**

[10] Woodsen M and Liu J 2006 Guided growth of nanoscale conducting polymer structures on surface-functionalized nanopatterns *J. Am. Chem. Soc.* **128** 3760-3

[11] Kemp N T, McGrouther D, Cochrane J W and Newbury R 2007 Bridging the gap: Polymer nanowire devices *Adv. Mater.* **19** 2634-8

[12] Das A, Lei C H, Elliot M, Macdonald J E and Turner M L 2006 Non-lithiographic fabrication of PEDOT nano-wires between fixed Au electrodes *Organic Electronics* **7** 181-7

[13] Noy A, Miller A E, Klare J E, Weeks B L, Woods B W and DeYoreo J J 2002 Fabrication of luminescent nanostructures and polymer nanowires using dip-pen nanolithography *Nano Lett.* **2** 109-12

[14] Huang S C and Glicksman M E 1981 Fundamentals of dendritic solidification–II Development of sidebranch structure *Acta Metall.* **29** 717-34

[15] Huang S C and Glicksman M E 1981 Fundamentals of dendritic solidification *Acta Metall.* **29** 701-15

[16] Langer J S 1980 Instabilities and pattern formation in crystal growth *Rev. Mod. Phys.* **52** 1-28

[17] Ivantsov G P 1947 Temperature field around spherical, cylindrical and needle-shaped crystals which grow in supercooled melt *Dokl. Akad. Nauk USSR* **58** 567

[18] Mullins W W and Sekerka R F 1964 Stability of a planar interface during solidification of a dilute binary alloy *J. Appl. Phys.* **35** 444-51

[19] Hwang R Q, Schroder J, Gunther C and Behm R J 1991 Fractal growth of two-dimensional islands: Au on Ru(0001) *Phys. Rev. Lett.* **67** 3279-82

[20] Saito Y, Goldbeck-Wood G and Müller-Krumbhaar H 1987 Dendritic crystallization:numerical study of the one-sided model *Phys. Rev. Lett.* **58** 1541-3

[21] Grier D, Ben-Jacob E, Clarke R and Sander L M 1986 Morphology and microstructure in electrochemical deposition of zinc *Phys. Rev. Lett.* **56** 1264-7

[22] Sawada Y, Dougherty A and Gollub J P 1986 Dendritic and fractal patterns in electrolytic metal deposits *Phys. Rev. Lett.* **56** 1260-3

[23] Kessler D A, Koplik J and Levine H 1988 Pattern selection in fingered growth phenomena *Adv. Phys.* **37** 255-339

[24] Langer J S and Müller-Krumbhaar H 1978 Theory of dendritic growth-I. Elements of a stability analysis *Acta Metallurgica* **26** 1681-7

[25] Saito Y 1996 *Statistical Physics of Crystal Growth* (River Edge: World Scientific)

[26] Cheng C, Gonela R K, Gu Q and Haynie D T 2005 Self-assembly of metallic nanowires from aqueous solution *Nano Lett.* **5** 175-8

[27] Thapa P S, Barisci J N, Yu D J, Wicksted J P, Baughman R and Flanders B N 2008 Directional growth of conducting polypyrrole and polythiophene nanowires *Appl. Phys. Lett.* **Submitted**

[28] Bockris J and Reddy A K N 1973 *Modern Electrochemistry* (New York: Plenum Press)

[29] Nelson P 2004 *Biological Physics* (New York: W. H. Freeman and Company)

[30] Boas M L 1983 *Mathematical Methods in the Physical Sciences* (New York: John Wiley & Sons)

[31] Zangwill A 1988 *Physics at Surfaces* (New York: Cambridge University Press)

CHAPTER IV

METHODOLOGY FOR INTRODUCING CELL-TO-WIRE CONTACTS

Abstract

Dictyostelium cells, long known to undergo cathodic electrotaxis,[22] are shown to attach themselves to the tips of submicron wires that are biased with a negative potential. There is a -42 mV voltage-threshold for wire-cell attachment, with negligible probability across the 0 to -38 mV range but probability that approaches 0.7 across the -46 to -100 mV range. It is pivotal that these contacts be made in a reproducible manner, without any skilled operator and less chance of perturbation of cells.

IV.1 Introduction

Animal cells are enclosed by a cell membrane, which separates the interior of the cell from its environment. The surface of the cell membrane consists of many channels, whose individual properties can be determined from current-voltage characteristics. Cell membrane is interfaced through microprobe or micropipette for the electrophysiological studies of the cells. The patch clamp technique invented by Neher and Sakmann is the widely used tool for the electrophysiological study of cells.[1] It provides a voltage clamp measurement of ionic current in individual channel of cell membrane.[1, 3] In this

technique, the microtip of the glass pipette (diameter of ~1μm) is attached to the membrane and a small section of it is sucked out. It has been important tool for studying cellular processes. However, there is high risk of rupturing the membrane during mechanical interfacing to the cell and need a skilled operator to perform this operation. Hence, there is high enthusiasm to develop an alternative soft contact process of cells.

Integration of nanotechnology with experimental biology has great significance in the current biological research fields and has received tremendous attention these days. The wire-cell contact is the pivotal part of this work. The study reported in chapters II and III establishes the DENA-based growth of conducting polymer nanowires in on-chip circuitry. These materials are well-suited for attaining wire-cell contacts. To execute this goal, we employ the social amoebae *Dictyostelium discoideum.* These cells are able to grow at room temperature, and to be processed for electrochemical assays without sophisticated equipment.

IV.2 Experimental Setup

Figure IV.1a depicts the experimental apparatus for inducing electrotaxis and executing the soft cell-to-wire contact process. The optical micrograph depicts an electrode array that is typical of those used in this study. These arrays were deposited on 0.5 mm thick quartz substrates, using standard photolithographic techniques. A 500 nm thick layer of Au was deposited on top of a 100 nm thick base layer of Ti. The deposited metal was annealed by exposing the chip to 420 ^{o} C argon atmosphere in a tube furnace

for 10 min, strengthening the electrodes against electrochemical degradation during wire-growth.

The wedge-shaped lithographic electrodes taper to tips that are ~ 2 μm in width. However, visualization of cell-electrode junction process is improved by adding more finely structured metallic tips to the existing electrodes. This is readily done via the *directed electrochemical nanowire assembly technique* that we have recently developed.[5, 6] Briefly, a 5 μl drop of 55 mM aqueous indium acetate [$In(CH_3COO)_3$] solution was deposited over the electrode gap. A 1.0 MHz square wave signal with amplitude of ±18 V was routed from a function generator (Hewlett Packard, 8111A) through a voltage amplifier (FLC Electronics, F10A), was applied to the left electrode while the right electrode was grounded. A 690 nm diameter crystalline indium wire then grows along the tip-to-tip line across the electrode gap at a velocity of 37 μms^{-1}: as reported elsewhere, the wire-diameter and growth velocity are precisely specified by the frequency of the alternating voltage.[4] After the growth step, the electrodes are cleaned by wicking away the salt solution and gently rinsing with distilled H_2O for 3 times.

Type KAx3 *Dictyostelium discoideum* cells were grown on glass substrates that were immersed in HL-5 culturing medium at 24 ^oC according to standard protocols.[38] Depriving these cells of their food source significantly enhances their migratory behavior, particularly electrotaxis. Thus, the cells were separated from the HL-5 medium (which contains cAMP) by centrifuging a 1000 μl volume of the cell-medium suspension for ~20 sec at 5000 rpm. The precipitated cells were washed by discarding the excess HL-5

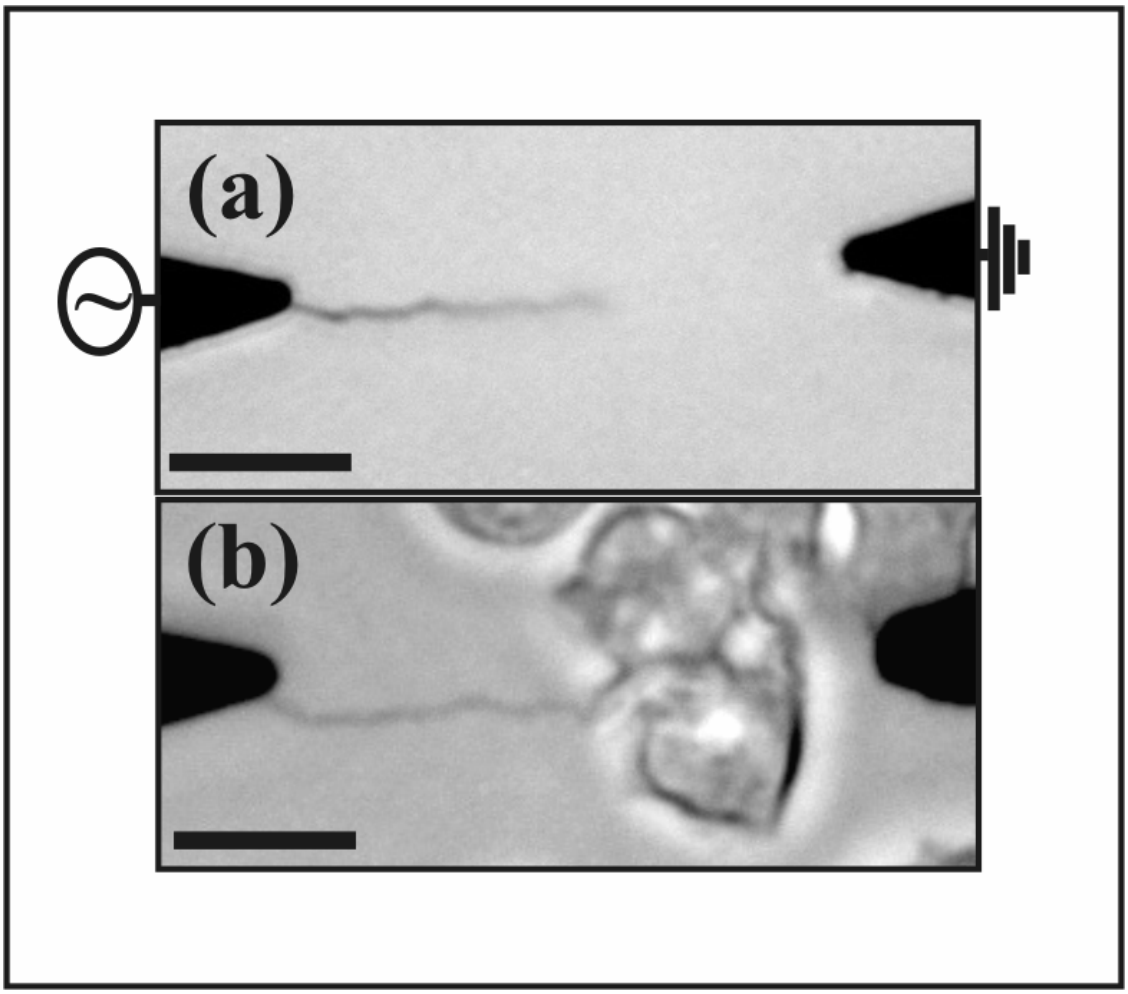

Figure IV.1 (a) The DENA apparatus for growing metallic nanowires. The optical micrograph shows a wire grown half way across the gap from aqueous indium acetate [$In(CH_3COO)_3$] solution. **(b)** The process of cell-to-wire attachment by inducing cell with -70 mV bias applied to the left electrode. The scale bars represent 10 μm.

medium, adding 1000 μl volume of 12 mM phosphate buffer to the vial containing the cells, then gently shaking them for 1 minute. This process was twice-repeated before suspending the cells a final time in 200 μl of phosphate buffer, which does not contain cell nutrient. After holding the cells in the buffer solution for 5-6 hours, the starved cells were deposited on the array by ejecting a 10 μl volume of the cell-suspension over the electrode gap. After ~20 minutes, the cells had typically attached to the glass substrate and were actively migrating.

Electrotaxis was induced by using a source meter (Keithley, 2400) to apply a steady -50 mV potential to the sharp-tipped (left) electrode while grounding the other electrode. This process is depicted in the series of snapshots that are shown in Figure IV.2. Figure IV.2a depicts the initial configuration of cells as they are migrating about on the electrode-array. This image was captured at the time of application of the steady voltage (*i.e.* at $t = 0$ s). There is no contact between the wire and the cell, as the distance-of-closest-approach between the wire-tip and the nearest cell is ~2.5 μm. However, 30 s after the voltage was turned on, the central cell has extended a pseudopod to contact the biased wire, as shown in Figure IV.2b. At $t = 60$ s, the cell has migrated so that a ~2 μm section of its side is in contact with the wire, as shown in Figure IV.2c, and at $t = 90$ s the cell has enveloped the tip of the wire (see Figure IV.2d). This series of images shows that the cell establishes contact with the sharp tip of the negatively biased electrode. The migration of cells towards negatively biased electrodes is normal cathodic electrotaxis and is expected of *Dictyostelium* cells.[33] However, the attachment of the cell to the tip of the biased electrode has, to our best knowledge, not previously been reported.

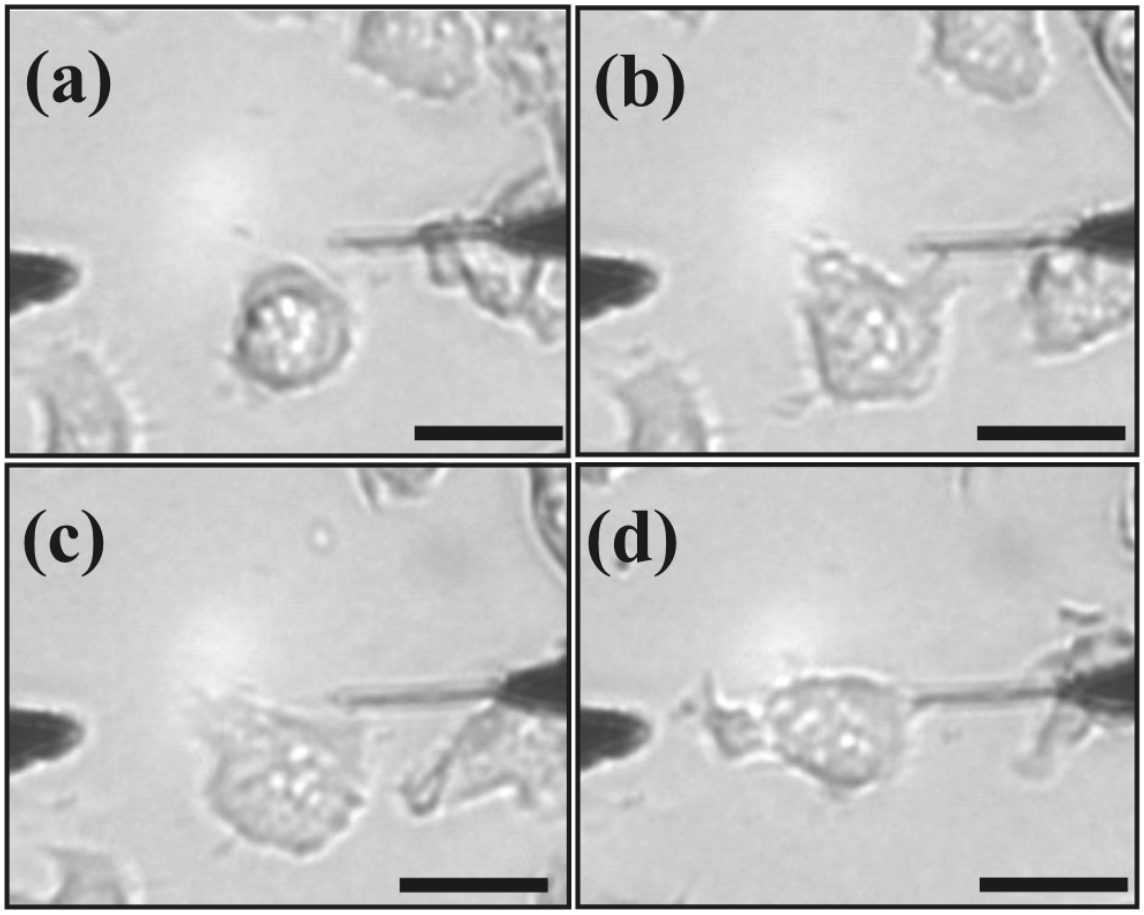

Figure IV.2: Image of an electrode array with an indium wire grown half way across the gap with a -50 mV bias applied to the right electrode. The sequence of images collected at **(a)** 0 s, **(b)** 30 s, **(c)** 60 s, and **(d)** 90 s demonstrates a *Dictyostelium* cell attaching itself to the negatively biased wire. The scale bar represents 10 μm.

In this approach of cell-to-wire attachment, the user does not manually force the wire into contact with the cell, which could harm the cell. Rather, the cell itself moves into contact with the cell, which is non-invasive approach to achieve wire-cell contact. This extraordinary behavior of cells provides a technique to develop a soft contact process of cell-wire attachment avoiding the potentially difficult task of the user adequately contacting the cell. This wire-cell contact process is quite reproducible.

IV.3 Threshold Voltage for Wire-Cell Attachment

To better understand the parameters governing this process, we have characterized the attachment-probability as a function of the applied voltage as shown in Figure IV.3. The probability for a given voltage was determined as follows. Cells were cultured onto an electrode array as described above. Only populations with cellular densities between 50 cells/mm^2 and 70 cells/mm^2 were used in this study. A single trial consisted of applying a voltage to the modified electrode (while grounding the other) and observing the system for 10 minutes to see if a cell attached itself to the biased wire. If attachment occurred and was maintained (*i.e.* the cell did not crawl away) during this period, a probability-value of 1 was assigned to the trial; otherwise, a probability-value of 0 was assigned to that trial. 10 trials were made for each voltage, and the mean and the standard deviation of the mean for the 10 probability-values were computed. These probability-determinations are plotted as the filled circles in Figure IV.3, while the standard deviations are represented by the error-bars in this plot. This data-set is rather extensive with 25 different voltages studied across the 0 to -100 mV range.

The data are well fit by a sigmoidal curve with a point of inflection at -42 mV. There is negligible probability for attachment across the 0 mV to -38 mV range, whereas there is significant probability for attachment (approaching 0.7) across the -46 mV to -80 mV range. (The maximum observed probability is less than 1.0 because there is always a probability that attachment will not occur during the finite waiting period). Thus, this study reveals a voltage threshold of -42 mV to wire-cell attachment. There is a high degree of sample-to-sample reproducibility associated with this process: in obtaining the probability data for the 42-100 mV range in Figure IV.3 (*i.e.* the range where attachment occurs) a cell was observed to attach itself to a biased wire 67 times out of the total of 100 trials that were made in characterizing that range.

It falls beyond the scope of this letter to determine the physiological response in the cell that is induced by the -42 mV stimulus. However, it is of potential relevance that the membrane potential of starved *Dictyostelium* cells has been measured to be -39 mV, [28] which compares well with the -42 mV threshold-value determined here. A reasonable expectation is that the wire-cell attachment process requires the stimulation of voltage-gated ion channels in plasma membranes of *Dictyostelium* cells. Future investigations will test this hypothesis.

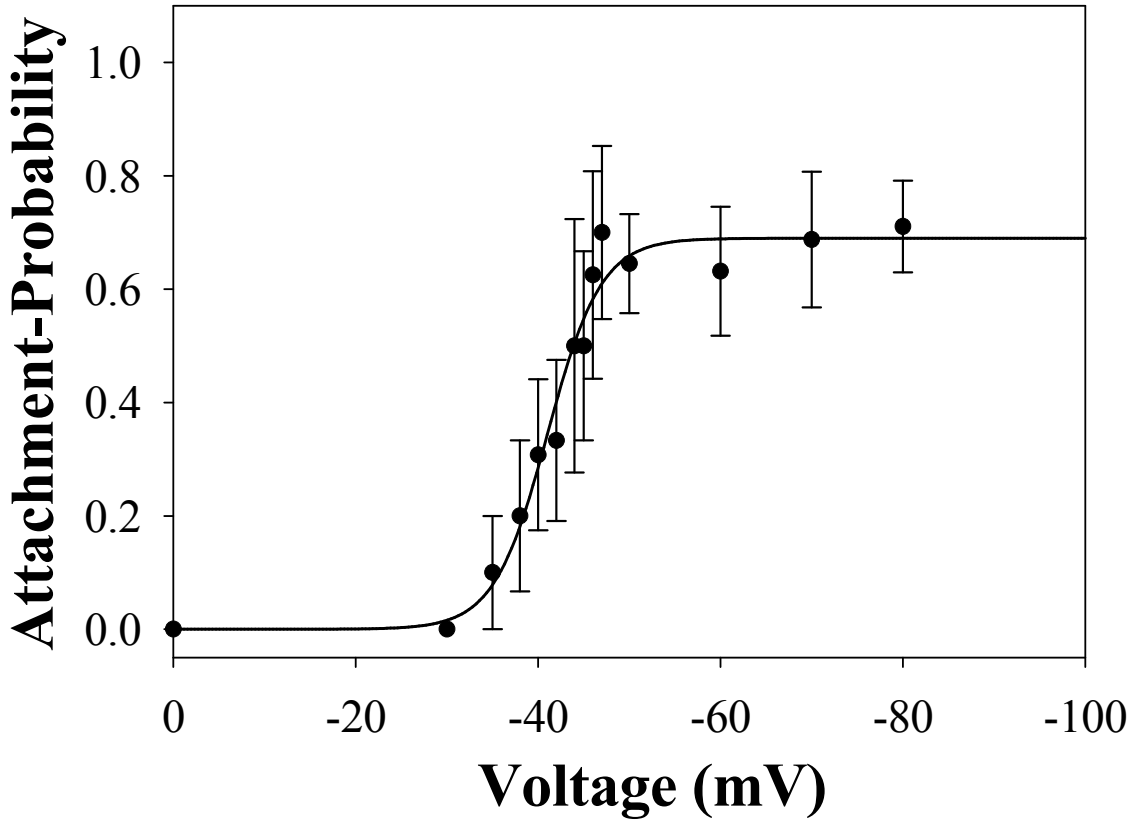

Figure IV.3: A plot of cell-to-wire attachment probability versus the steady voltage applied to the biased electrode. The sigmoidal curve transitions at -42 mV.

IV.4 Cell Viability

To test the healthiness of cells during the cell-wire attachment process by elctrotactical behavior of *Dictyostelium* cells, we have compared the change in shape of the cell as depicted in Figure IV.4. Figure IV.4a and IV.4c illustrates the cells cultured at 12 mM phosphate buffer solution, whereas Figure IV.4 b and IV.4d illustrates the cells after they made a contact with negatively biased wire. Figure IV.4c-d depicts population of cells to which an agonist has been added.

We characterized the shape of the cells as a function of time as depicted in Figure IV.5. The rounding of the cell generally characterizes the unhealthiness or stressed condition of *Dictyostelium* cells. The shape of the cells were analyzed based on roundness parameters of the cell.

$$= \frac{(\quad)^2}{4(\quad)} \qquad \text{(IV.1)}$$

The roundness parameter = 1 for circular cells and >1 for healthy, amoebic cellular shapes.

Nine successive images with more than 20 cells in the field of view at a time delay of 10 sec were analyzed and the mean for ~20 roundness values were computed for each time. These mean values are plotted as a function of time in Figure IV.5; the standard deviations are represented by the error bars in this plot. In Figure IV.5, the solid line corresponds to the cell population to which the voltage was applied in order to

induce cell-to-wire attachment. This line fluctuates about a roundness value of ~2.5 for the entire experiment. Thus, these cells maintain their amoebae shapes and remain healthy during the cell-to-wire attachment process. In contrast, the dashed line corresponds to the cell population to which the agonist was added. This line decays from a value of 3.0 to unity in 30 sec. Thus, these cells round up due to stress.

The plot signifies that there is not considerable change in the shape of the *Dictyostelium* cells on the process of cell-to-wire attachment. Thus, this study reveals that this technique of cell-to-wire attachment has much less chance of perturbing the cells in comparision to other user enforced methods.

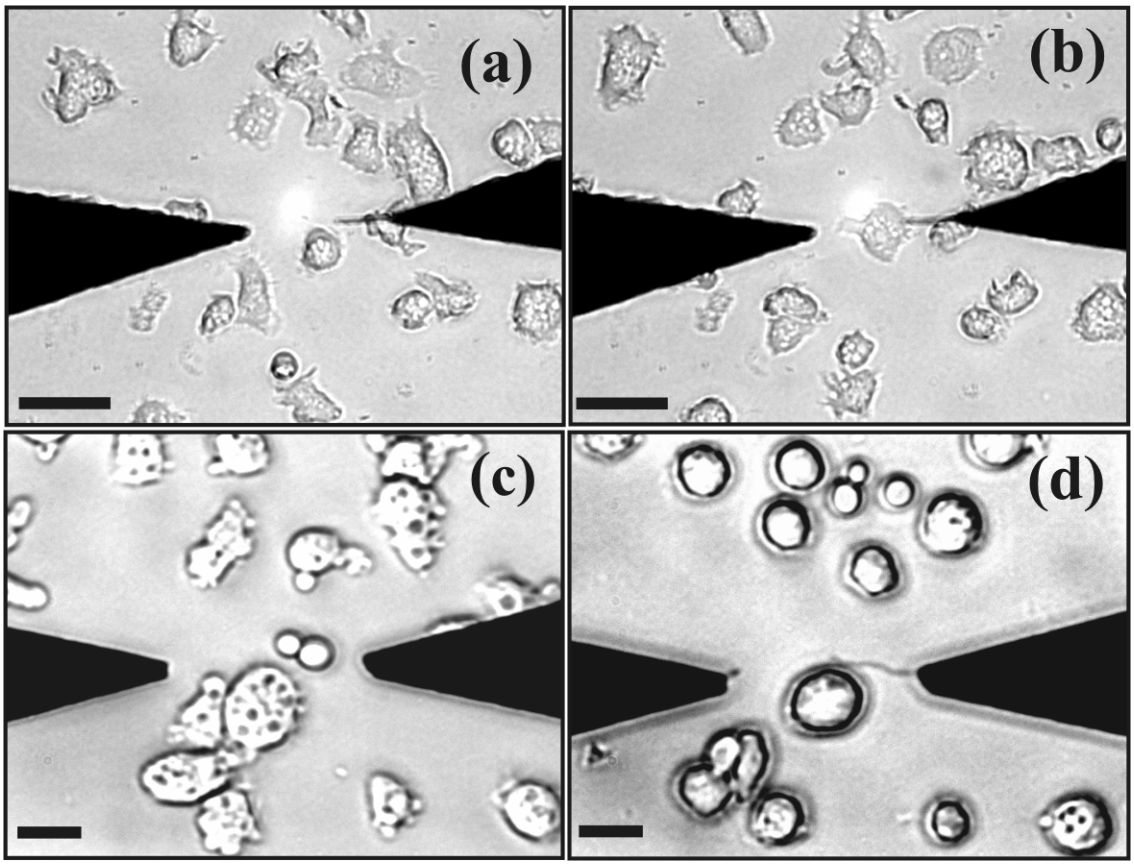

Figure IV.4: (a) Image of an electrode array with an indium wire grown approximately half way across the gap with *Dictyostelium* cells deposited on it. **(b)** 136 s later demonstrates a *Dictyostelium* cell attached to the -50 mV biased wire. **(c)** *Dictyostelium* cells that are cultured onto an electrode array. **(d)** A polythiophene wire grown from the right electrode in close proximity to the live cell; the voltage applied is switched to steady -70 mV and image is collected after 136 s of wire-cell attachment. The scale bars for Figures **(a) & (b)** represent 20 μm and **(c) & (d)** represent 10 μm.

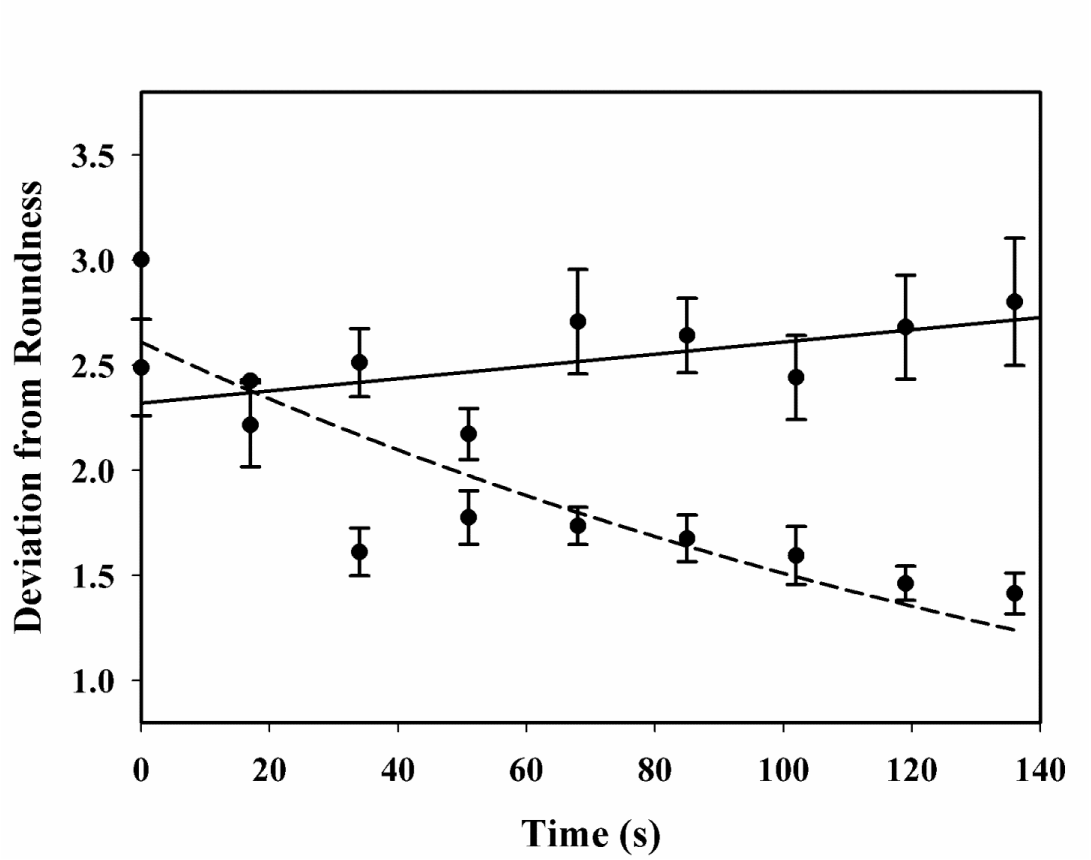

Figure IV.5: A plot of deviation from roundness of cell versus the time. Cell-to-wire attachment process by inducing the migration of cells on phosphate buffer by -70 mV at DENA grown wire (solid lines) and addition of an agonist (Indium salt solution) to the cells (dashed lines).

IV.5 Results & Discussions

Our preliminary studies showed that when a steady -50 mV signal is applied locally via a DENA grown wire, the targeted cell closest to the wire generally attaches itself to the wire as shown in Figure IV.2. In this approach, the user does not manually force the wire into contact with the cell as in the classical patch clamp techniques. Rather, the cell finds the wire and chooses for itself how to make contact. This soft contact process of wire-cell attachment only weakly perturbs the cells, as no external force is applied to the cell. During several repetitions of these experiments, the process of self cell-wire attachment is observed repeatedly. From the analysis of roundness of the cell, it is illustrated in Figure IV.5, the cells were still healthy at electric stimulation of -50 mV by DENA grown wire. From the sigmoidal plot in Figure IV.3, the wire-cell attachment voltage is transitioning at -42 mV, which is essentially the membrane potential of a *Dictyostelium discoideum* cell.

IV.6 Conclusions

This technique can be an alternative approach for cell-to-wire contact. It has potential to preserve the characteristics of the living cells and maintain the motility of the cells. The cell-wire attachments could be made in a reproducible manner, without any skilled operator and with less chance of perturbation of cells.

REFERENCES

1. Neher, E. & Sakmann, B., "The patch clamp technique," *Sci. American*, 44-51 1992).

2. Lipp, P. & Niggli, E., " A hierarchical concept of cellular and subcellular Ca^{2+} Signaling," *Prog.Biophys. Mol. Biol*., **65**, 265-296 (1996).

3. Bruce, A., Johnson, A., Lewis, J., Raff, M., Roberts, K. & Walter, P. (Molecular Biology of the Cell, 2002).

4. Ozturk, B., Talukdar, I., & Flanders, B. N., "Directed growth of diameter-tunable Nanowires", *Nanotechnology* **18 (***2007).*

5. Talukdar, I., Ozturk, B., Mishima, T. D. & Flanders, B. N., "Directed Growth of Single-Crystal Indium Wires". *Applied Physics Letters*, 2006, **88**: p. 221907.

6. Ozturk, B., Mishima, T. D., Grischkowsky, D. R. & Flanders, B. N., "Single-Step Growth and Low Resistance Interfacing of Gold Nanowires". *Nanotechnology 2007.* **18**: p. 175707.

7. Bockris, J. & Reddy A. K. N. (Modern Electrochemistry, Plenum Press, New York, 1973).

8. Nelson, P. (Biological Physics, W. H. Freeman and Company, New York, 2004).

9. Yoshida, K,. & Soldati, T., "Dissection of Amoeboid Movement into Two Mechanically Distinct Modes" *Journal of Cell Science* **119**: 3833-3844 (2006).

10. Kunito, Y., & Thierry, S., *Journal of Cell Science* **119:** 3833-3844 (2006).

11. Sasaki, T., A., Firtel, A., *European Journal of Cell Biology* **85:** 873-895 (2006).

12. Zho, M., Jin, T., McCaig, C., D., Forrester, J., V., & Devreotes, P., N., *The Journal of Cell Biology* **157:** 921-927 (2002).

13. Azhar, M., Manogaran, P., S., Kennady, P., K., Pande, G., & Nanjundiah, V., *Experimental Cell Research* **227:** 344-351 (1996).

14. Yumira, S., Furuya, K., & Takeuchi, I., *Journal of Cell Science* **109:** 2673-2678 (1996).

15. Richardson, S. M., Hendricks, J. L., & Martin D. C., "Electrochemical Polymerization of Conducting Polymers in Living Neural Tissue". *J. Neural Eng.* **4** (2007): L6-L13.

16. Ouyang, J., Chu, C. W., Chen, F. C., Xu, Q., & Yang, Y., "High-Conductivity PEDOT: PSS Film and Its Application in Polymer Optoelectronic" *Adv. Funct. Mater.,* **15:** No. 2 (2005).

17. Laporte, C., Kosta, A., Klein, G., Aubry, L., Lam, D., Tresse, E., Luciani, MF., & Golstein, P., " A Necrotic Cell Death Model In a Protist" *Cell Death and Differentiation*, **14:** 266-274 (2007).

18. Charest, G. P., & Firtel, R. A., " Feedback Signaling Controls Leading-Edge Formation During Chemotaxis" *Current Opinion in Genetics & Development*, **16:** 339-347 (2006).

19. Franca-Koh, J., Kamimura, Y., & Devereotes, P., "Navigating Signaling Networks: Chemotaxis in Dictyostelium discoideum", *Current Opinion in Genetics & Development*, **16:** 333-338 (2006).

20. Kim, J., Van Haastert, P., & Devreotes, P. N., " Social Sciences: G-Protein Coupled Receptor Signaling Pathways in Dictyostelium discoideum", *Chemistry & Biology*, **3:** 239-243 (1996).

21. Keizer-Gunnink, I., Kortholt, A., & Van Haastert, P. J. M.,"Chemoattractants and Chemorepellents act by Inducing Opposite Polarity in Phospholipase C and PI3-Kinase Signaling", *The Journal of Cell Biology*, **177:** 579-585 (207).

22. Zhao, M., McCaig, D. C., Agius-Fernandez, A., Forrester, J. V., & Araki-Sasaki, K., "Human Corneal Epithelial Cells Reorient and Migrate Cathodally in a Small Applied Electric Field", *Current Eye Research*, 1997.

23. Kim, D. H., Richardson-Burns, S. M., Hendricks, L., Sequera, C., & Martin, D. C. "Effect of Immobilized Nerve Growth Factor on Conductive Polymers: Electrical Properties and Cellular Response", *Adv. Funct. Mater.* **17:** 79-86 (2007).

24. Richardson-Burns, S. M., Hendricks, J. L., Foster, B., Povlich, L. K., Kim, D. H., & Martin D. C., "Polymerisation of The conducting Polymer Poly (3,4-ethylenedioxythiophene) (PEDOT) Around Living Neural Cells", *Biomaterials,* **28:** 1539-1552 (2006).

25. Zheng, G., F., Patolsky, F., Cui, Y., Wang, W., U., & Lieber, C., M., *Natl. Biotechnol.* **23:** 1294-1301 (2005).

26. Hahm, J., & Lieber, C., M., *Nano Lett.* **4:** 51-54 (2004).

27. Parent, C., A., & Devreotes, P., N., *Science* Vol: **284** (1999).

28. Van, D., J., Ypey, D. L., & Van der Molen, L. G., "Electrophysiological properties Of Dictyostelium derived from membrane potential measurements with micro-Electrodes". *J. Membr. Biol.* **106:** 123-134 (1988).

29. Firtel, A., R., *Genes & Development* **9:** 1427-1444 (1995).

30. Patolsky, F., B. P. T., Yu, G., Fang, Y., Greytak, A. B., Zheng, G., & Lieber, C. M., "Detection, Stimulation, and Inhibition of Neuronal Signals with High-Density Nanowire Transistor Arrays." *Science*, **313:** 1100-1104 (2006).

31. Zho, M., Bai, H., Wang, E., Forrester, J. V., & McCaig, D. C., "Electrical Stimulation Directly Induces pre-Angiogenic Responses in Vascular Endothelial Cells by Signaling Through VEGF Receptors." *Journal of Cell science,* **117:** 397-405 (2004).

32. McCaig, D. C., Rajnicek, A. M., Song, B., & Zhao, M., "Controlling Cell Behavior Electrically: Current Views and Future Potential." *Physiol Rev,* **85:** 943-978 (2005).

33. Shanley, L. J., Walczysko, P., Bain, M., MacEwan, D. J., & Zhao, M., "*Influx of extracellular Ca^{2+} is necessary for electrotaxis in Dictyostelium,*" J. Cell. Sci., **119**, 4741-4748 (2006).

34. Thapa, P. S., Barisci, J. N., Yu, D. J., Wicksted, J. P., Hadwiger, J. A., Baughman, R. H., & Flanders, B. N., "Directional Growth of Conducting Polypyrrole and Polythiophene Wires" *Appl. Phys. Lett.* Submitted (2008).

35. Britto, P., Santhanam, K., & Ajayan, P., *Bioelectrochem. Bioenerg.,* **41:** 121 (1996).

36. Chen, R., Bangsaruntip, S., Drouvalakis, K., Wong, N., Kam, S., Shim, M., Li, Y., Kim, W., Utz, P., & Dai, H., *PNAS* **100:** 4984 (2003).

37. Fei, S., Chen, J., Yao, S., Deng, G., He, D., & Kuang, Y., *Anal. Biochem.,* **339:** 29 (2005).

38. Watts, D. J., & Ashworth, J. M., "Growth of Myxameobae of the Cellular Slime Mould Dictyosteium inAxenicCuure," *The Biochemical Journal,* **119:** 171-174 (1970).

CHAPTER V

MEASUREMENT OF SUB-CELLULAR FORCE

Abstract

Migrating cells exert forces against the substrate for forward movement. *Dictyostelium discoideum* migrates in a particular direction in response to chemical gradient as well as electrical gradient by the extension of pseudopodia. Protrusion of a leading edge rely on forces generated by actin polymerisation. Here, we report the preliminary application of simple nanotechnology for the measurement of forces exerted at single adhesive contact-points of individual *Dictyostelium* cells by measuring the displacements of the cantilevered nanowires grown by *Directed Electrochemical Nanowire Assembly* (DENA) technique.

V.1 Introduction

The *Dictyostelium discoideum*, amoeba is an excellent model system for the study of cell migration. Growing amoeba chemotaxes toward folic acid and other kind of nutrients, whereas starved cells respond to cyclic AMP.[1, 2] The amoeba cells also respond to DC electric field by electrotaxis, which is a fundamental process for healthy animal tissues. The signaling mechanism of chemotaxis has been well understood, but

further study is needed before beneficial intervention in the electrotactical process will be possible.[3, 4] The DENA grown nanowire can be a potential approach to elucidate this mechanism by correlating the forces that are exerted at the individual adhesive contacts (between cell and the wire substrate) with signaling and cytoskeletal dynamics inside the cell. Because the area of the tip can tuned to 0.5 μm^2 (or even less),[12, 13] the probability of it being in contact with only one adhesion complex on the cell-surface is significant: a typical contact-density is 0.5 contacts/μm^2.[8] Measurements that resolve forces from individual parts of the cell-especially individual adhesive contacts-are still quite difficult to make.[5, 9] The most widely employed approach consists of observing the cell-induced motion (i.e. wrinkling or marker-displacement) of a deformable substrate;[5] because the substrate is continuous, a substantial modeling-effort is required to correlate the substrate displacement-field with the discrete set of adhesive contact-points and associated force-vectors.[6] Moreover, direct measurement of the force exerted at a single adhesive contact-point has to our best knowledge, yet to be accomplished (although some relevant work has come close).[8]

Previous work by other groups and researchers had highlighted a technique for direct measurement of the mechanical forces exerted by single cell or multiple cells by the use of flexible substrate.[10] The methods of recording the deformation of flat elastic substrata has been widely used, but the method of detection of forces through independent microfabricated elastic cantilever beam has not been used to date. Therefore, there is considerable enthusiasm for developing simple and precise probes of

subcellular forces because the capability would enable elucidation of interesting migratory mechanisms, such as electrotaxis.

The present study reports a new aspect of electrotaxis: individual *Dictyostelium* cells are induced to migrate towards and attach themselves to flexible polymer wires that carry a steady -70 mV bias. The attachment is made with a single pseudopod, and the elastic deflection of the wire provides direct information on the force exerted by the pseudopod. Thus, this work establishes a new method for measuring subcellular forces with little influence of the other parts of the cell.

V.2 Materials and Methods

The experimental layout of this force-probe is shown in Figure V.1a-b. Figure V.1a depicts a polythiophene nanowire grown from the tip of the left lithographic electrode by *directed electrochemical nanowire assembly* (DENA), a technique that we developed for adding metallic[13, 14, 15] and conducting polymeric nanowires to lithographic circuitry.[12] A 5 μl volume of 10 mM solution of 3,4-ethylenedioxythiophene (EDOT) with 20 mM concentration of poly styrene sulfonate (PSS) made with 12 mM concentration of phosphate buffer solution was deposited across the gap of the electrodes. A ±3 V square wave signal at 100 KHz frequency was applied to one of the electrodes with the other electrode grounded through a function generator (Hewlett Packard, 8111A). The radical-cation polymerization may be initiated upon the electrochemical generation of some active species at the tip of the electrode, followed by the rapid

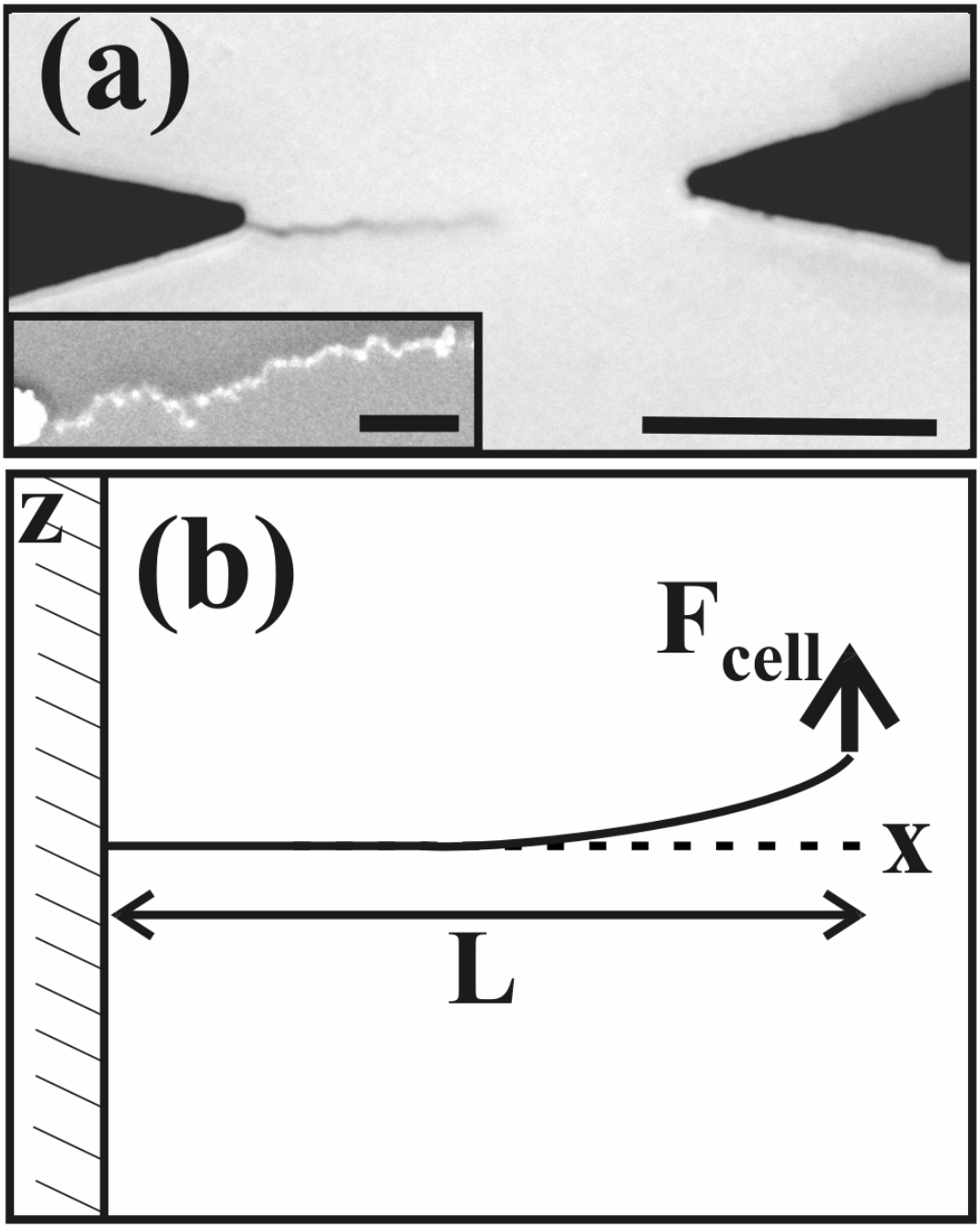

Figure V.1: **(a)** An optical micrograph of a polythiophene wire grown from aqueous thiophene-poly styrene sulfonate solution via the DENA technique. The scale bar denotes 10 μm. Inset: An SEM micrograph of a polythiophene wire. The scale bar denotes 3 μm. **(b)** A schematic of a deflected cantilever F_{Cell} acting at a distance L along its length.

polymer chain growth as the wire grows across the gap. The wire-growth voltage is terminated when the polythiophene wire has grown to the half-way point in the electrode gap. The flexibility of the polymer wire enables cell-induced deflections from its equilibrium position to be observed on an optical microscope. One end of the wire is attached to the electrode while the other is free, surrounded only by the phosphate buffer solution. Thus, the elastic behavior of the wire is well-described by that of a cantileverd rod.[19] This model is depicted in Figure V.1b.

The inset depicts a scanning electron micrograph (SEM) of the wire; its length-wise averaged diameter is 380 nm. The flexibility of the polymer wire enables cell-induced deflections from its equilibrium position to be observed on an optical microscope. The wire may be modeled as a cantilevered beam of length L (Figure V.1b):[16] thus, when a force F_{App} is applied to a point at a distance L along the length of the rod, the rod deflects by a distance z(L) that is proportional to F_{App}. This response is described by the equation,

$$F_{App} = 3YI\frac{z(L)}{L^3} \qquad \text{(V.1)}$$

Where, Y is Young's modulus for the beam-material, and I is the second cross sectional moment of the rod.[16] A cylindrical bulk polythiophene beam has a Young's modulus of 10.0 GPa[18] and a moment of $\pi R^2/4$, where R is its radius.[17] With knowledge of these properties, measurement of z(L) and L for the cantileverd polythiophene wire determines the force applied by the attached cell, F_{App}.

A 10 µl volume of starved KAx3 *Dictyostelium* cells cultured at 12 mM concentration of phosphate buffer is deposited across the electrode gap shown in Figure V.1a, we then allowed 15 minutes for the cells to settle down and attach to the glass substrate. A series of images depicting cell-induced deflection of the wire is shown in Figure V.2 a-c. Figure V.2a depicts the initial configuration of a 15.4 µm long polythiophene wire which extends roughly halfway across the 30 µm wide electrode gap, and the live *Dictyostelium* cells. The wire and the nearest cell are not yet in contact, with their distance-of-closest approach being 2.3 µm. A -70 mV bias is then applied to the left electrode by a source meter (Keithley 2400) to induce cell-to-wire attachment. Figure V.2b captured 30 s after voltage-application, depicts the cell with a pseudopod in contact with the tip of the biased wire. The contact point is at the tip, 15.4 µm along the length of the wire. An enlarged view of the wire-cell contact region is shown in the inset; the dashed white outline, which denotes the undeflected position from the wire of panel (a), ovelaps well with the wire's position in panel (b). However, Figure V.2c captured 70 s later, shows that in migrating to a new position while maintaining contact with the biased tip, the cell has deflected the wire. This displacement is evident in the inset where the new position of the wire lies to a large extent outside of the dashed white outline that denotes the equilibrium wire-position. From this view, the tip of the wire is seen to have deflected by an amount $z(L) = 1.3$ µm in the vertical direction. This displacement of wire due to the force exerted by the extension of pseudopds in *Dictyostelium* cell is an evidence of strong mechanical contact established between wire and cell.

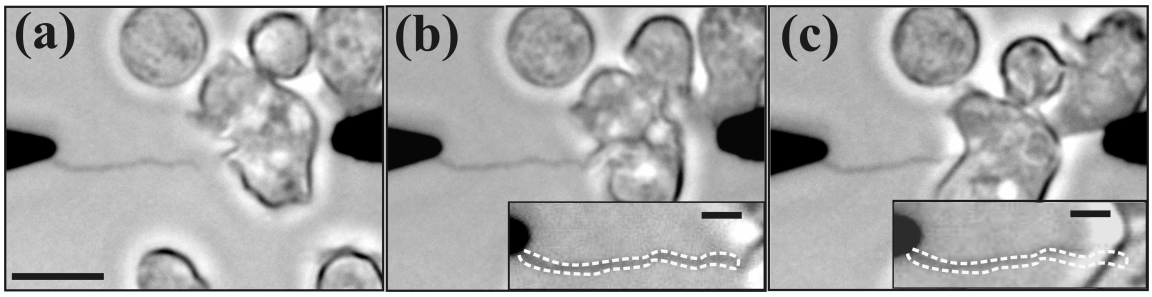

Figure V.2. A series of images showing the response of the *Dictyostelium* cells to a steady -70 mV bias that is applied to the flexible polymer wire. **(a)** The equilibrium position of the wire before voltage is applied. **(b)** 46 s after applying the voltage. The inset shows a magnified view of the wire, where the white dashed outline denotes the wire-position in panel (a). **(c)** 70 s after applying the voltage. The inset compares the wire-position in panel (a) (white dashed line) to the deflected wire-position. The scale bar in panel (a) denotes 10 μm, and the scale bars in the insets denote 3 μm.

V.3 Results

Invoking the equation $F_{App} = 3YI\frac{z(L)}{L^3}$ enables calculation of the vertical-component of force exerted by the cell on the cantilevered wire.[16] Modeling the wire as a polythiophene cylinder with Y = 10 GPa and R = 190 nm, and measuring L = 15.4 μm and z(L) = 1.3 μm in Figure V.2 c, F_{App} is found to be 12 nN; the 4 other force-determination that we have made using this technique range from 5 nN to 20 nN. These values compare reasonably well with the 4-7 nN forces generated by the individual lamellipodium of fibroblasts but measured by a more time-intensive lithographic patterning approach.[8]

V.4 Conclusions

In this study, we presented a new approach for probing subcellular forces. This work establishes a new method for measuring subcellular forces exerted at single adhesive contact-points of individual cells with little influence of the other parts of the cell. Thus, this capability will constitute a simple tool for resolving poorly understood migratory mechanisms of living cells, such as electrotaxis.

REFERENCES

1. Zho, M., Jin, T., McCaig, C., D., Forrester, J., V., & Devreotes, P., N., *The Journal of Cell Biology* **157:** 921-927 (2002).

2. Hadwiger, J. A., "Developmental Morphology and Chemotactic Responses are Dependent on Gα Subunit Specificity in Dictyostelium," Developmental Biology **312:** 1-12 (2007).

3. Zho, M., Bai, H., Wang, E., Forrester, J. V., & McCaig, D. C., "Electrical Stimulation Directly Induces pre-Angiogenic Responses in Vascular Endothelial Cells by Signaling Through VEGF Receptors." *Journal of Cell science,* **117:** 397-405 (2004).

4. McCaig, D. C., Rajnicek, A. M., Song, B., & Zhao, M., "Controlling Cell Behavior Electrically: Current Views and Future Potential." *Physiol Rev,* **85:** 943-978 (2005).

5. Harris, A., Wild, P., & Stopak, D., "Silicone Rubber Substrata: A New Wrinkle in The Study of Cell Locomotion" *Science* **208:** 177-179 (1980).

6. Harris, A., Stopak, D., & Wild, P. "Fibroblast Traction as a Mechanism for Collagen Morphogenesis" *Nature* **290:** 249-251 (1981).

7. Schwarz, S., U., Balaban, Q., N., Riveline, D., Bershadsky, A., Geiger, B., & Safran, A., S., " Calculation of Forces at Local Adhesions from Elastic Substarte Data: The Effect of Localized Force and the Need for Regularization" *Biophysical Journal* **83:** 1380-1394 (2002).

8. Galbraith, G., C., & Sheetz, P., M., "A Micromachined Device Provides a New Bend on Fibroblast Traction Forces" *Proc. Natl. Acad. Sci*. **94:** 9114-9118 (1997).

9. Wolgemuth, W., C., "Force and Flexibility of Flailing Myxobacteria" *Biophysical Journal* **89:** 945-950 (2005).

10. Barentin, C., Sawada, Y., & Rieu, J. P., "An Iterative Method to Calculate Force Exerted By Single Cells and Multicellular Assemblies from the Detection of Deformations of Flexible Substrates." *Eur. Biophys. J.* **35:** 328-339 (2006).

11. Pierres, A., Benoliel, M., A., Bongrand, P., & Merwe, V., A., P., "Determination Of the Lifetime and Force Dependence of Interactions of Single Bonds Between Surface-Attached CD2 and CD48 Adhesion Molecules" *Proc. Natl. Acad. Sci.* **93:** 15114-15118 (1996).

12. Thapa, P. S., Barisci, J. N., Yu, D.J. et al., "Directional Growth of Conducting Polypyrrole and Polythiophene nanowires," *Appl. Phys. Lett.* **Submitted** (2008).

13. Ozturk, B., Talukdar, I., & Flanders, B. N., "Directed growth of diameter-tunable Nanowires", *Nanotechnology* **18,** 365302 **(***2007).*

14. Talukdar, I., Ozturk, B., Mishima, T. D., Grischkowsky, D. R. & Flanders, B. N., "Directed growth of single crystal indium wires". *Appl. Phys. Lett.* **88**: 221907 (2006).

15. Ozturk, B., Mishima, T. D., Grischkowsky, D. R. & Flanders, B. N., "Single-Step Growth and Low Resistance Interfacing of Gold Nanowires". *Nanotechnology* **18**: 175707 (2007).

16. Feynman, P., R., Leighton, B., R., Sands, M. (The Feynman Lectures on Physics, Addison-Wesley Publishing Company, California, 2005).

17. Boas, L., M. (Mathematical Methods in the Physical Sciences, John Wiley & Sons Inc., New York, 1983).

18. Shu, X., & Feng, X., Q.," Effects of Thickness on Mechanical Properties of Conducting Polythiophene Films" *J. Of Material Science Letters* **21:** 715-717 (2002).

19. Landau, L. D., & Lifshitz, E. M. (Theory of Elasticity, Oxford, Butterworth-Heinemann, 2000).

CHAPTER VI

CONCLUSIONS AND FUTURE DIRECTIONS

VI.1 Summary of Results and Conclusions

The series of the projects covered in this work represents a systematic study on growth of nanowires from variety of metallic and polymeric solutions. These nanowires are used as electrodes for the development of an alternative approach of cell-to-wire contact with weak perturbation to cells. As described in chapter II and III, we have demonstrated the directed growth of metallic and polymeric nanowires by a technique that is called *Directed Electrochemical Nanowire Assembly* (DENA). This technique enables the template-free single-step growth and interconnecting of the wires with targeted points in external circuitry. The experimental results illustrate that nanowires grow in specified directions across distances of ~100 μm. The experimental results in Figure III.5 (a)-(f) clearly demonstrates the wire growth between the user-chosen pair of electrodes, despite lots of other chances to grow wire by nearby electrodes.

The structure that is produced by the DENA technique ranges from needle-shaped wires to highly branched tree-like deposits. The diffusion limited dendritic growth and the anti-correlation between the velocity and tip-radius of the wire suggests that dendritic solidification underlies the DENA technique. It has been established that directional

growth is a natural feature of dendritic solidification. For the materials with crystalline anisotropy, the dendrite grows in the direction that is normal to the crystallographic plane with the largest surface energy. The resulting structures, having large area-sides with small surface energies and small area tips with large surface energies is consistent with the dependence on crystalline anisotropy and reveals directional growth to be a natural feature of dendritic solidification.

In contrast, we have demonstrated in chapter II, the DENA technique may be used to grow conducting polymeric wires along predictable, inter-electrode paths. Polymeric materials are amorphous and, therefore, lack crystalline anisotropy, so this behavior is unexpected. A transmission electron micrograph of a polypyrrole wire-segment and polythiophene wire-segment showed a knobby structure, resembling the individual branches of a fractal aggregates, which indicates the diffusion limited aggregation. This structural similarity suggests that the DENA fabricated wires also grow by diffusion limited aggregation. A typical micro-Raman spectrum is shown in Figure II.2a and Figure II.2b for such a wire. The film spectrum agrees well with the wire-spectrum. This close correspondence implies that the DENA-grown wire is composed of polypyrrole and polythiophene. From the current-voltage (I-V) profiles of the ploypyrrole and polythiophene electrode-wire-electrode assemblies, the conductivities of the individual polypyrrole and polythiophene wires were calculated as shown in table II.1. The average conductivity of polypyrrole wire material is calculated as 0.5 ± 0.3 S cm^{-1} and polythiophene wire material is calculated as 7.6 ± 0.8 S cm^{-1}.

These polymeric wires are amorphous materials with zero crystalline anisotropy, whose natural tendency is to grow non-directionally. However, it is observed that the DENA induces these wires grow directionally across 10s-of-microns distances. Thus the hypothesis is that the directional character of the DENA technique is due to the externally applied voltage. From the plot of Figure III.5, it is observed that the fraction of V_{app} that is not screened but instead extends across the entire electrode gap. In light of these analytical results, we conclude that there is a reasonable amount of potential to grow the wire to a long range between a pair of electrodes. The one dimensional diffusive model that was analyzed in Figure III.6 supports this hypothesis, as the wire growth will occur along the vector describing the ridge of electric field maxima in the inter-electrode region.

We have chosen *Dictyostelium* discoideum amoeba for our study, as these cells are able to grow at room temperature, and to be processed for electrochemical assays without sophisticated equipment. *Dictyostelium* cells have ability of directional sensing. These cells chemotax in the gradient of chemical stimulants and electotax to the gradient of electric fields. The mechanism of signaling pathway in chemotaxis is well understood, however the mechanism of signaling pathway in electrotaxis of *Dictyostelium* cell still needs to be understood.

It has demonstrated that, the cells were viable at lower concentration of EDOT : PSS solution prepared on cell culture medium. The directed wire could grow at the solution prepared on phosphate buffer and could control the growth of wire by adjusting

the applied voltage and frequency. We have demonstrated in Figure II.4b, the capability of DENA technique to grow a polymeric nanowire to a targeted point on the live cell. It has demonstrated the ability to grow the wire on cell cultured medium, however the motility of the cells is reduced and the cells were more rounded in shape. This observation reveals that, the cell are somewhat affected by the wire-growth condition (salt concentration, growth voltage) associated with DENA technique. In addition to this during the interfacing of the wire to the cell membrane, there is still higher chances of rupturing the cell membrane.

In order to reduce the chances of cell perturbation during wire-cell interfacing, we have exploited the electrotactical behavior of *Dictyostelium discoideum* cells. It induced a self contact to negatively biased nanowire as illustrated in Figure IV.3a-d. A nanowire is grown half-way across the electrode gap, cleaned the solution and cultured the cells above the DENA grown wire electrodes. It is observed that, the *Dictyostelium* cells start to forage for food and ultimately find the negatively biased wire, migrates to its tip and make a self cell-to-wire contact as shown in Figure IV.3b. The user does not manually force the wire into contact with the cell, which could harm the cell. Rather, the cells find the wire by migration and make a cell-wire attachment by itself. This electrotactical behavior of cells provided a technique to develop a soft contact process of cell-to-wire contact avoiding the potentially difficult task of the user adequately contacting the cell. It is observed that the cell–wire attachment could be performed in a reproducible manner, without any skilled operator and with less chance of perturbation of cells. With the analysis of the shape of the cell, Figure IV.5 illustrates the shape of the cells remain

stable during the cell-to-wire attachment process. This demonstrates that cells remain healthy and viable during the self cell-to-wire contact process.

We have determined the threshold voltage for cell–wire attachment. Initially, when no voltage is applied to the wire, the cells do not perform electrotaxis and do not make a wire-cell attachment. Several readings were recorded for various DC Voltages applied to the nanowire through a source meter. An average of ten observations for each voltage is taken. From a plot of wire-cell attachment probability vs the voltage amplitude in Figure IV.2a, –42 mV is determined as the threshold voltage for wire cell attachment, which is essentially the membrane potential of *Dictyostelium* cell.

The polythiophene wire grown by DENA technique illustrated in Figure V.2 has demonstrated flexiblibility and elastic properties. The *Dictyostelium* cells migrated to the negatively biased polythiophene wire made a strong electrical contact. During the extension of the pseudopods, it is observed that the pseudopds exerted a small force to the wire pulling or pushing the wire away from the neutral axis. This bending or displacement of wire signifies the elastic properties of the wire. It is an evidence of strong electrical contact established between wire and cell. By the application of Hooke's law, the force exerted at the individual adhesive contacts between cell and substrate by single *Dictyostelium* cell is calculated, which is in the order of ~10 nN.

In conclusion, this work demonstrates the capability of DENA grown nanowire as an alternative approach for cell-to-wire contact with weak perturbation to cells. We have

demonstrated the reproducibility of self cell-wire attachment at the membrane potential of *Dictyostelium* cells. It is demonstrated the electrotaxis of individual cell and multiple interfacing of an individual cell to pair of electrodes.

VI.2 Future Directions

DENA grown conducting polymer wires were employed in interfacing to live cell membranes. With self cell-wire attachment, known as soft contact process, there is much less chances of perturbation to cells. The voltage-stimulation of the cells with this technique has potential to study the electrophysiological processes. The mechanism of signaling pathway in electrotaxis of *Dictyostelium* cells still need to be understood. With the demonstration of the capability of DENA grown wire to measure the forces exerted at single adhesive contact-points of individual cell, a tool could be developed for precise probing of subcellular forces. This could enable to resolve the poorly understood migratory mechanisms of living cells, such as electrotaxis.

VITA

Prem Thapa

Candidate for the Degree of

Doctor of Philosophy

Dissertation: METHODOLOGY FOR THE DIRECTIONAL GROWTH OF CONDUCTING NANOWIRES AND THEIR ATTACHMENT TO LIVE CELLS.

Major Field: Photonics

Biographical:

Personal Data: Born in Syangja, Nepal on June 16, 1971, son of Mr. Purna S. Thapa and Mrs. Bhagawoti Thapa.

Education: BS in Electrical Engineering from Bangladesh Institute of Technology, Rajshahi, Bangladesh in Jan, 1995. MS in Electrical Engineering from Oklahoma State University, Stillwater, Oklahoma in Dec 2002. Completed the requirements for the Doctor of Philosophy in Photonics at Oklahoma State University, Stillwater, Oklahoma in December, 2008.

Experience: Research Assistant, Oklahoma State University in Dept. of Physics August 2004 to May 2008 , Teaching Assistant August 2001 to August 2004, Research Assistant at Dept. of Electrical Engineering, January 2000 to August 2001. Lecturer at Institute of Engineering, Kathmandu , Nepal in Dept. of Electrical Engineering, May 1995 to Dec 1999.

Professional Memberships:
Materials Research Society
American Physical Society
Nepal Engineers Association

Name: Prem Thapa Date of Degree: December, 2008

Institution: Oklahoma State University Location: Stillwater, Oklahoma

Title of Study: METHODOLOGY FOR THE DIRECTIONAL GROWTH OF CONDUCTING NANOWIRES AND THEIR ATTACHMENT TO LIVE CELLS.

Pages in Study: 99 Candidate for the Degree of Doctor of Philosophy

Major Field: Photonics

Scope and Method of Study: The purpose of this study was to develop a technique as an alternative approach for establishing cell-to-wire contact by the use of nanowire grown from *Directed Electrochemical Nanowire Assembly* (DENA) technique with weak perturbation to living cells.

Findings and Conclusions:

Methodology for the long-range growth of metallic and polymeric nanowires between on-chip electrodes has been established. Theoretical modelling reveals that there is a strong, long-range component of the applied potential that extends entirely across the gap between a user-chosen pair of electrodes. This component defines a vector of maximum ion-flux in the laboratory reference frame. For the metallic nanowires, this voltage-component tends to bring the crystallographic axis of growth into coincidence with the flux vector. For the polymeric nanowires, this channel of maximum ion flux restricts polymerization to the channel-region. Hence, amorphous materials may be grown with wire-like geometries, and the growth-path of the wires may be controlled. These wire-laden chips are useful substrates for cell physiological studies. To this end, the electrotactical behavior of *Dictyostelium discoideum* cells has been exploited to induce the formation of strong mechanical contacts between individual pseudopodia and the tips of biased polymeric wires in a manner that is only weakly perturbative to the cells. This capability is expected to facilitate electro-mechanical probing of cellular processes.

ADVISER'S APPROVAL: Dr. Bret N. Flanders